2008

Bio-Signal Analysis in Fatigue and Cancer Related Fatigue;Weakening of Corticomuscular Functional Coupling

Qi Yang
Cleveland State University

BIO-SIGNAL ANALYSIS IN FATIGUE AND CANCER RELATED FATIGUE: WEAKENING of CORTICOMUSCULAR FUNCTIONAL COUPLING

Qi Yang

Bachelor of Engineering in Instrumentation

Shanghai Jiao Tong University

June, 1999

Master of Engineering in Instrumentation

Shanghai Jiao Tong University

March, 2002

Submitted in partial fulfillment of requirements for the degree

DOCTOR OF ENGINEERING IN APPLIED BIOMEDICAL ENGINEERING

at the

CLEVELAND STATE UNIVERSITY

August, 2008

To my family for their love and support

ACKNOWLEDGEMENTS

First of all, I wish to express my deepest gratitude and respect for my advisor, Dr. Guang H. Yue, whose expert guidance and constant encouragement made it possible for me to present this thesis. He was always there to provide the best possible facilities, collaborations, opportunities and challenging tasks to build a concrete foundation for my future goals. My research aptitudes have been tremendously enhanced over the years working with him.

I would like to thank my co-adviser Dr. George Chatzimavroudis in Chemical and Biomedical Department of Cleveland State University and Dr. Brain Davis, Ms. Becky Laird, Ms. Darlene Montogomery in Applied Biomedical Program at Cleveland State University for their professional help over the years.

It was a valuable experience to collaborate with Dr. Meller Davis and Dr. Dilara Khoshknabi in Taussig Cancer Center, Cleveland Clinic and Dr. Xiaofeng Wang in Department of Quantitative Health Sciences, Lerner Research Institute, Cleveland Clinic. Thanks for their insightful suggestions and generous help.

I would like to thank Dr. George Chatzimavroudis，Dr. Fuqin Xiong，Dr. Jingzhi Liu and Dr. Andrew B. Slifkin for serving as members of my dissertation committee and their valuable time, helpful comments and suggestion for my proposal and my thesis research.

I would like to thank Dr. Jingzhi Liu and Dr. Vlodek Sieminow for their help and guidance in starting my research in Dr. Yue's group. I also wish to express my deepest thanks to all of my colleagues and friends whose friendship and encouragement have made my experience at Cleveland Clinic and Cleveland State University a memorable

one. In particular, I would like to thank Dr. Luduan Zhang, Dr. Bing Yao, Dr. Ying Fang, Dr. Didier Allexandre and Mr. Vinoth Ranganathan, Dr. Katarzyna Kisiel-Sawjewicz, Mr. Zhiguo Jiang, Ms. Alexandria Wyant, Mr. Venkateswaran Rajagopalan in the Neural Control of Movement Laboratory for their helpful input and stimulating discussions regarding my research, thesis writing and their invaluable friendship.

Last but not least, I want to express my deepest gratitude to my parents Longdi Shen and Yihao Yang, my husband Xi Chen for their endless love, unconditional support, and countless sacrifices.

BIO-SIGNAL ANALYSIS IN FATIGUE AND CANCER RELATED FATIGUE: WEAKENING OF FUNCTIONAL CORTICOMUSCULAR COUPLING

QI YANG

ABSTRACT

Fatigue is a common experience that reduces productivity and increases chance of injury, and has been reported as one of most common symptoms with greatest impact on quality-of-life parameters in cancer patients. Neural mechanisms behind fatigue and cancer related fatigue (CRF) are not well known. Recent research has shown dissociation between changes in brain and muscle signals during voluntary muscle fatigue, which may suggest weakening of functional corticomuscular coupling (fCMC). However, this weakening of brain-muscle coupling has never been directly evaluated. More important information could be gained if fCMC is directly detected during fatigue because a voluntary muscle contraction depends on integration of the entire chain of events and is a complex interaction of different components from the central nervous system to peripheral systems. This research, first, evaluated the effect of muscle fatigue on fCMC in healthy people by determining electroencephalography (EEG)-electromyography (EMG) coherence during two stages of a sustained voluntary muscle contraction, one with minimal fatigue and the other with severer fatigue. The obtained results suggest that despite an elevation of the power for both the EEG and EMG activities with muscle fatigue, the fatigue weakens strength of fCMC between the two signals. Secondly, given

the fact that there is larger discrepancy between central and peripheral fatigue in CRF, the effect of cancer related fatigue on fCMC was evaluated by comparing EEG-EMG coherence during a muscle fatigue task in CRF patients with healthy controls. CRF patients showed significantly lower fCMC compared to healthy controls during minimal fatigue stage which may be caused by possible pathophysiological impairments in the patients. Finally, to better understand dynamic fatigue effect on fCMC, a single trial coherence estimation based on Morlet wavelet was developed and applied to investigate fatigue effect on fCMC in single trial during repetitive maximal muscle contractions. It was revealed that the decreasing pattern of the fCMC varied among the subjects but the overall decreasing trend was consistent across subjects. The results from the single-trial study suggest it is possible to detect more dynamic fCMC adaptations under acute neuromuscular instability conditions, such as muscle fatigue.

This research reveals that muscle fatigue impairs normal coupling between the central and peripheral neuromuscular systems, which could be a major factor contributing to worsened performance under fatigue influence. In general, cancer patients with fatigue symptom exhibit substantially weakened fCMC, even without influence of muscle fatigue. The findings are potentially important in understanding neural mechanisms of muscle fatigue and cancer related fatigue, and in guiding development of new methodologies to improve diagnosis and treatment of fatigue symptoms in clinical populations.

TABLE OF CONTENTS

LIST OF TABLES

LIST OF FIGURES

CHAPTER I

INTRODUCTION

1.1 Fatigue and Cancer Related Fatigue

Muscle Fatigue has been defined as "any exercise-induced reduction in the ability to exert muscle force or power, regardless of whether or not the task can be sustained." (Bigland-Ritchie and Woods, 1984). It can result from one of the following muscle activities: maintaining sustained/repetitive submaximal muscle contractions against a given load, or maintaining sustained/repetitive maximal muscle contractions. With submaximal (>25% maximal level) voluntary contraction, the progressively increasing amplitude and decreasing frequency power of the electromygram (EMG) activity and the increasing effort to sustain the same force output are the typical markers of fatigue. In the case of maximal muscle contraction, the gradually decreasing amplitude and frequency power of the EMG activity, reduction of the force output and eventually inability to maintain the maximal force are signs of fatigue (Bigland-Ritchie, 1981, Enoka and Stuart,

1992, Taylor et al., 2000). Fatigue reduces productivity, lowers quality of life and increases chances of injury. The consequences are more severe in cancer patients with the fatigue symptom. Fatigue has been reported as the greatest impact on quality-of-life parameters in cancer patients (Dimeo et al., 1997, Stone et al., 1998, Barnes and Bruera, 2002).

Different from normal fatigue, cancer related fatigue (CRF) is a persistent subjective sense of tiredness that interferes with daily activities (Mock et al., 2000). It comes on suddenly, does not result from activity or exertion, and is not relieved by rest or sleep. It might continue even after treatment is complete. A universal definition for cancer-related fatigue does not exist (Davis, Khoshknabi and Yue 2006). The National Consortium of Cancer Centers' definition of CRF is "an unusual persistent subjective sense of tiredness related to cancer or cancer treatment that interferes with usual function" (Mock et al. 2000). In the US, there are more than 8 million cancer survivors, and more than a million new cancers are diagnosed each year (Holley, 2000). Cancer and its treatment cause a variety of symptoms such as pain, decreased appetite, mouth ulcers, hair loss, nausea and vomiting, shortness of breath, a general deterioration of physical condition, and fatigue. Of these symptoms, fatigue has been ranked the longest lasting and most disruptive symptom by cancer patients, affecting up to 70% of the patients after chemo- and radiotherapy; fatigue also has the greatest impact on quality-of-life parameters (Dimeo et al., 1997; Stone et al., 1998; Barnes and Bruera, 2002). The prevalence of fatigue was as high as 96% when patients received chemotherapy with radiotherapy (Irvine et al., 1991). Although fatigue is a highly prevalent condition among

patients with cancer, mechanisms that contribute to CRF are very poorly understood (Review: Wu and McSweeney, 2001).

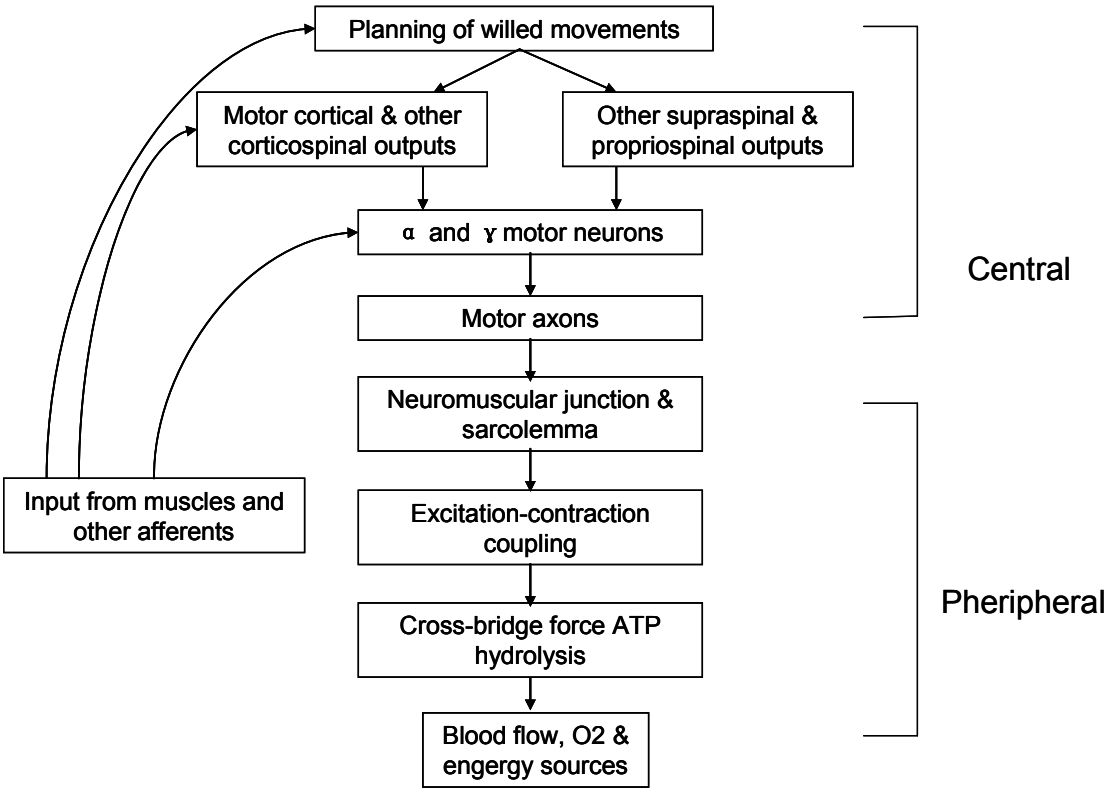

Fig.1.1. Illustration of motor pathway of physical activities (Gandevia, 2001, 81:1725-1743).

Previous studies on muscle fatigue have been focused on all levels of the motor pathway (Fig. 1.1), from muscle to brain, before, during and after fatigue motor task. Peripheral changes within the muscle associated with fatigue have been thoroughly studied, which included measurements made on single fibers, motor units and whole muscle (Taylor et al., 2000). The mechanisms of force loss (a major indication of muscle fatigue) on excitation-contraction coupling, the buildup of metabolic by-products and decreased efficiency of the contractile mechanism (Bigland-Ritchie et al., 1986, Balestra et al., 1992, Babcock et al., 1995), impaired sarcoplasmic Ca^{++} release and reuptake,

abnormal changes of the muscle fiber membrane (Abdelmalki et al., 1997) and impaired function of neuromuscular junction (Fuglevand et al., 1993) have been reported to be related to fatigue. Recently, it was found that these peripheral changes are not the only changes associated with the muscle fatigue and do not account for all fatigue-induced decreases in maximal voluntary muscle force. Some central factors from spinal and supraspinal levels have been reported to associate to or account for muscle fatigue. During a sustained submaximal muscle contraction, brain activation level increases measured by functional MRI (Liu et al., 2003, van Duinen et al., 2007) and motor-related cortical potential (MRCP) (Johnston et al., 2001) as fatigue sets in. The power in some frequency bands decreases in EEG signals with fatigue induced by maximal muscle contractions (Liu et al., 2005). In addition, shift of brain activation center (Liu et al., 2007) and decreased functional connectivity in the motor cortex (Peltier et al., 2005) have been found in muscle fatigue. A number of studies applied transcranial magnetic stimulation over human motor cortex during sustained maximal or submaximal contractions demonstrated reduced excitatory input from the motor cortex to fatiguing muscle (Taylor and Gandevia, 2001, Sogaard et al., 2006). Inhibitory interneurons and/or firing of fatigue-sensitive muscle afferents that act upon the corticospinal neurons would also inhibit voluntary descending drive to muscle during fatigue (Bigland-Ritchie, 1981, Leonard et al., 1994, Belhaj-Saif et al., 1996, Taylor et al., 2006). Effects of muscle fatigue on almost each site of the motor control pathway from peripheral to central have been investigated separately, however, the relationship of these changes on various sites has never been directly addressed. A muscle contraction depends on integration of the entire chain of events and is a complex interaction of different sites from the peripheral to

central systems. Yet, many studies reported discrepancies between fatigue at muscular and supraspinal levels. It would be interesting to directly examine functional coupling changes between the brain and muscle during fatigue, which would provide additional information to the whole picture of fatigue mechanism. For CRF, although fatigue is a highly prevalent condition among patients with cancer, there have been no studies to date that have reported CRF-related cortical potentials or changes in frequency of EEG-measured brain signals, or CRF-related brain function adaptations in neuroimaging investigation.

1.2 Coherence

Both cortical and muscular oscillatory activities have been known as common physiological signals and have been suggested to be the mechanism of synchronizing the information related to the same function in different neuronal populations (Mima and Hallett, 1999). These corticomuscular oscillatory activities can be quantified by EEG and EMG signal analysis in frequency domain. The synchronization of the signals in the brain and muscle is suggested as functional corticomuscular coupling (fCMC). This functional coupling is frequently measured by cross-correlating EEG and EMG signals in frequency domain, known as coherence. Coherence is mathematically bounded between 0 and 1, where 1 means two signals are perfectly linearly correlated at a given frequency and 0 means no correlation at all. A widely used method of calculating coherence is based on smoothed cross-spectrum and auto-spectrum of the fast Fourier transform (FFT) averaged on numerous non-overlapping signal segments.

The strength of fCMC during voluntary motor actions was first systematically estimated by calculating coherence between magnetoencephalography (MEG) recorded from the scalp and surface EMG of the first dorsal interosseous muscle (Conway et al., 1995). It is now generally accepted that corticomuscular coherence reflects communications between the brain and muscle, which is considered to be related to controlling force (Kilner et al., 1999, Feige et al., 2000, Kilner et al., 2000, Marsden et al., 2000), and the communications are thought to be mainly mediated by the direct corticospinal pathway (Mima and Hallett, 1999). Significant coupling between signals of the brain and muscle mainly at beta (15-35 Hz) frequency band during voluntary motor performance has been reported in healthy subjects, either in EEG-EMG (Kristeva et al., 2007) or MEG-EMG coherence studies (Conway et al., 1995, Kilner et al., 2000). Abnormal features of fCMC have been reported with the coherence measurements in movement disorders, such as stroke (Mima et al., 2001), tremor (Volkmann et al., 1996, Hellwig et al., 2000) and Parkinson's disease (Salenius et al., 2002), suggesting impairments in corticomuscular communication in the patients.

1.3 Thesis purpose

Given the significance of the fCMC measurement in understanding motor control mechanisms and paucity of knowledge related to neuromuscular mechanisms behind fatigue and CRF, it is expected to gain important information by applying coherence analysis to neuromuscular signals in fatigue and CRF study. This dissertation had three main objectives: to quantify normal fCMC change during voluntary muscle fatigue in healthy subjects; to detect abnormal fCMC in patients with cancer-related fatigue; to

explore a technique for detecting fCMC in single trial and providing and potentially making real time fCMC measurement. The fCMC was quantified by EEG-EMG coherence.

It was hypothesized that fatigue would weaken the strength of the corticomuscular coupling based on differential effects of fatigue on the central and muscular systems and the coupling would be further weakened due to the larger discrepancy between central and peripheral fatigue caused by pathophysiological impairment in CRF patients compared to healthy subjects.

1.4 Thesis Organization

First, since the fCMC during fatigue has never been directly investigated, it was evaluated in healthy people to learn the normal pattern of its change with fatigue (Chapter 2). Based on the normal changing pattern, the fCMC in CRF was assessed to identify the pathophysiological effect on the fCMC and its deviation from the normal pattern (Chapter 3). Furthermore, the single trial method of estimating fCMC and power spectrum based on wavelet transform was explored (Chapter 4) as the methods used in the first two studies did not provide satisfactory information regarding dynamic adaptation of the fCMC. In addition, this single trial method of estimating power spectrum was applied to develop an EEG-based brain computer interface (BCI) prototype (Chapter 5). This BCI system could potentially be used to control assisting devices for patients who are disabled. The last study (Chapter 5) was not related to fatigue, but the project was a one step forward in detecting motor related EEG signal pattern in real time

based on the same method described in chapter 4. Finally, Chapter 6 provides conclusions of the studies and discussion of future directions.

CHAPTER II

WEAKENING OF FUNCTIONAL CORTICOMUSCULAR COUPLING DURING MUSCLE FATIGUE

2.1 Introduction

Voluntary motor performance is a result of the cortical command driving muscle actions. Fatigue caused by prolonged voluntary muscle activities can be attributed to failure of the central or peripheral system. Accumulating evidence suggests contributions from both systems to muscle fatigue (for a review see Gandevia 2001), yet many studies reported discrepancies between fatigue at muscular and supraspinal levels. For example, the level of electromyogram (EMG) of the finger flexor muscles kept increasing during a sustained handgrip contraction at 30% maximal level, but the activity level of the primary motor cortex (measured by functional MRI) contralateral to the performing hand began to decline long before the subjects felt exhausted and terminated the contraction (Liu et al. 2003). Similar dissociation between signal alterations at muscular and supraspinal levels

has been observed during muscle fatigue induced by maximal voluntary contractions (MVC) (Gandevia et al., 1996, Butler et al., 2003, Liu et al., 2005, Liu et al., 2005). Furthermore, impairment of neuromuscular junction transmission function, especially with fatigue at low-intensity activity levels (Fuglevand et al., 1993, Fuglevand et al., 1995) and inhibitory feedback from the fatiguing muscle(s) to the output neurons at supraspinal levels (Garland, 1991, Garland and Kaufman, 1995) would likely complicate the input (from the brain) and output (muscle) relation and may further enlarge the corticomuscular dissociation. The unparallel changes of the signals between the muscle and central nervous system suggest decoupling of the two signals. However, this fatigue-related weakening of brain-muscle coupling has never been directly investigated. Understanding this phenomenon would help better elucidate fatigue mechanisms and develop therapies for treating the vast fatigue symptoms in clinical populations.

The strength of corticomuscular signal coupling during voluntary motor actions was first systematically estimated by calculating coherence between magnetoencephalography (MEG) recorded from the scalp and surface EMG of the first dorsal interosseous muscle (Conway et al., 1995). Although the physiological basis of corticomuscular coherence has been far from clear, it is now generally accepted that corticomuscular coherence reflects communications between the brain and muscle, which is considered to be related to controlling force and modulating fatigue (Kilner et al., 1999, Feige et al., 2000, Kilner et al., 2000, Marsden et al., 2000), and the communications are thought to be mediated by the direct corticospinal pathway (Mima and Hallett, 1999). Significant coupling between signals of the brain and muscle mainly at beta (15-35 Hz) frequency band during voluntary motor performance has been reported in healthy

subjects, either in electroencephalography (EEG)-EMG (Kristeva et al., 2007) or MEG-EMG coherence studies (Conway et al., 1995, Kilner et al., 2000). Abnormal features of corticomuscular coupling have been reported with the coherence measurements in movement disorders, such as stroke (Mima et al., 2001), tremor (Volkmann et al., 1996, Hellwig et al., 2000) and Parkinson's disease (Salenius et al., 2002), suggesting impairments in corticomuscular communication in the patients.

The purpose of this study was to evaluate the effect of muscle fatigue on functional corticomuscular coupling (fCMC) by determining EEG-EMG coherence during two stages of a sustained voluntary muscle contraction, one with minimal fatigue and the other with more severe fatigue. It was hypothesized that fatigue would weaken the strength of the coupling based on differential effects of fatigue on the central and muscular systems.

2.2 Methods

2.2.1 Subjects

Nine right-handed healthy subjects (48.2 ± 14.8 years, 3 men) participated in the study. The study was approved by the Institutional Review Board at the Cleveland Clinic. All subjects gave informed consent prior to their participation. All subjects performed a sustained contraction of the right-arm elbow flexors at 30% maximal level until subjective exhaustion. Elbow flexion force, surface EMG and multi-channel EEG were simultaneously recorded during the sustained contraction.

2.2.2 Data Recording

Sustained Contraction

The isometric sustained contraction was performed to fatigue the elbow flexor muscles (Fig.2.1). A target force of 30% maximal elbow flexion force was displayed on an oscilloscope using a horizontal cursor. (Maximal force was measured at the beginning of the experiment.) Participants matched the target with the exerted force in a sitting position with the elbow joint at ~100º and maintained the exerted force on the target until they felt exhausted and were no longer able to continue the contraction. Participants were verbally vigorously encouraged to continue the sustained contraction as long as possible. The sustained contraction was terminated if the exerted force dropped 10% or more for more than 3 s. The forces (maximal and sustained contraction) were measured by a force transducer (JR3 Universal Force-Moment Sensor System, Woodland, CA), acquired by a Spike2 data-acquisition system (1401 Plus, Cambridge Electronic Design, Ltd., Cambridge, UK), digitized at 100 samples/s, and stored on hard disk of a personal computer. The subjects maintained the contraction for an average of 461 ± 45s. But during the sustained contraction, the electrical stimulation-evoked twitch force was measured every 30 seconds to monitor the voluntary activation level of the biceps brachii. Stimulation electrodes were attached to the skin surface overlying the BB muscle. Supramaximal-intensity single electrical pulses (1-ms duration) were applied through a digital stimulator (Grass S8800) to evoke twitch force. This electrical stimulation was designed for another experiment purpose of comparing levels of voluntary activation between a group of patients with cancer-related fatigue and healthy controls. The EEG and EMG data with artifacts related to electrical stimulation was visually inspected and carefully excluded for the coherence analysis.

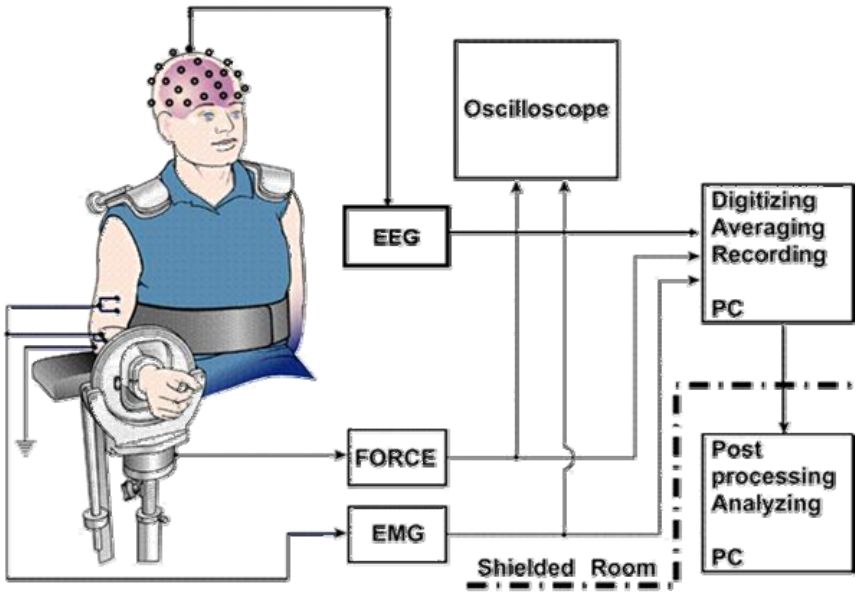

Fig. 2.1. Illustration of experiment setup

EMG Measurement

Bipolar surface EMG was recorded from the belly of the biceps brachii (BB), brachioradialis (BR) and triceps brachii (TB) muscles using Ag-AgCl electrodes (In Vivo Metric, Healdsburg, CA). Recording diameter of each electrode was 8 mm and center-to-center inter-electrode distance was ~3 cm. A reference electrode was placed on the skin overlying the lateral epicondyle near the elbow joint. The EMG signals were amplified (X1000); band-pass filtered (3 Hz – 1 KHz), digitized (2000 samples/s), acquired by the Spike2 system, and stored on hard disk of the personal computer. For the EEG-EMG coherence analysis, the EMG signals of the three muscles were re-sampled at 250 points/s, the same sampling rate applied to the EEG (see below).

Multi-Channel EEG Measurement

Scalp EEG signals (referenced to the central electrode [Cz]) were recorded continuously during the sustained contraction using a 128-channel EEG data acquisition system (Electrical Geodesics, Inc. Eugene, OR, USA). The 128 electrodes were arranged

in a hat-like net and connected to each other by nylon strings. The electrode net was applied to the head after it was soaked in the electrolyte consisted of one liter of distilled water added with 1.5 teaspoons of potassium chloride and a few drops of baby shampoo (EGI System 200 Technical Manual). A small piece of sponge in each electrode absorbed the liquid and served as connecting media between the scalp and electrode. An impedance map, based on impedance values of all the electrodes, was displayed on a computer monitor to inspect the quality of connection. If a particular electrode showed high impedance, adjustment (such as applying pressure or adding more water) was made to improve the connection. The EEG data recording did not begin until the impedance for all electrodes settles below 10,000 ohms. All channels of the signals were amplified (X75,000), band-pass filtered (0.01 -100 Hz), digitized (250 sample/s) and recorded on hard disk of a dedicated personal computer connected to the EEG acquisition hardware and software.

2.2.3 Data Processing and Analysis

During offline processing, the EEG signals were re-referenced to the average value of the 128-channel signals (excluded the outer-most electrodes) and high-pass filtered at 3 Hz; the EMG signals were resampled to 250 Hz and high-pass filtered at 10 Hz to minimize low-frequency baseline fluctuation before rectification. All signals, especially the EEG were inspected visually. Recordings with artifacts caused by events such as electrical stimulation (see below), eye blinks, head movements, and/or muscle activation in and near the head areas were excluded and the corresponding EMG signals discarded. The entire duration (148 ± 24 s) of the clean EEG and EMG recordings was then divided into the first half (stage 1 with minimal fatigue) and second half (stage 2 with severer

fatigue). Subsequently, the signals in each stage were segmented into artifact-free epochs (256 samples in each epoch) without overlapping (mean 148.5 epochs, ranging from 56 to 264 among the nine participants). (Note that the subjects maintained the contraction for 461 ± 45 s in the experiment but the duration of the data used for the coherence analysis was much shorter. This was because supramaximal electrical stimulation-evoked twitch force was measured every 30 seconds during the sustained contraction to monitor the voluntary activation level (VAL) of the biceps brachii. The electrical stimulation protocol was for a separate project that compared the VAL between a group of patients with cancer-related fatigue and healthy controls [subjects of this study]. The high-intensity stimuli produced substantial artifacts onto the EMG and EEG data. After removing the artifact contaminated data, the total amount of "clean" data analyzed, on average, were only 148 ± 24 s, which was too short to be segmented into more than two stages for high-quality coherence measurements.)

In each stage, autospectrum and crossspectrum of the EEG and rectified EMG were calculated with a 256-point fast Fourier transform with Hamming window. (It has been shown that rectification of the EMG alters EMG power spectrum but does not change EEG-EMG coherence; further, the rectification makes the coherence peaks more clear [Yao et al. 2007].) The coherence of the two signals was obtained from normalization of the crossspectrum: $C_{xy}^2(f) = \left|S_{xy}(f)\right|^2 / (S_{xx}(f) * S_{yy}(f))$, where $S_{xx}(f)$ and $S_{yy}(f)$ respectively represented the cross-trial smoothed autospectrum of the EEG and EMG signals, x and y , for a given frequency f ; and $S_{xy}(f)$ was the cross-trial smoothed cross-spectrum. The frequency resolution was 0.98Hz. Significance of the

coherence was determined based on the 95% confidence level (Rosenberg et al. 1989).

Due to the volume of information, especially the large number of EEG channels, the coherence values of EEG channels overlying sensorimotor function-related brain regions with each of the three muscles (BB, BR or TB) were grouped into five scalp areas for statistical comparisons (ten electrodes in each scalp area): left, right, frontal, central and parietal (Fig. 2.2). Crossing-stage comparisons were limited to the beta (15-35Hz) frequency band since most of the significant EEG-EMG coherence values were detected at the beta frequency band in both stages 1 and 2. The calculated coherence was Z-transformed by the arc hyperbolic tangent transformation to stabilize the standard deviation (Rosenberg et al., 1989). The transformation was as follows:

$$Z = \arctan h(\sqrt{C}) \times \sqrt{2L}$$

Where C is the coherence value and L is the number of epochs.

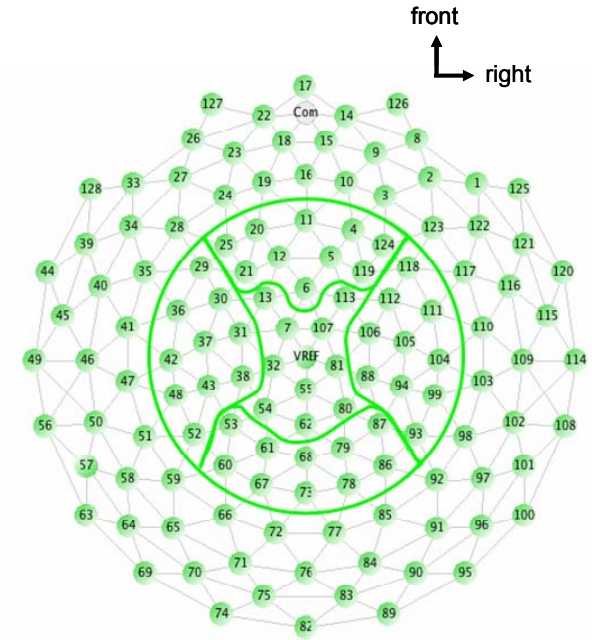

Fig. 2.2. Illustration of five scalp areas used for the statistical analysis of the EEG-EMG coherence: left, right, frontal, central and parietal areas.

The mean power of the beta band EEG in each scalp area and beta band EMG in each muscle at each stage was also calculated and normalized to the total power of stage 1. The total EEG power was the sum of the power computed from 3 to 50 Hz and the total EMG power frequency range was from 10 to 125 Hz (the EMG resampling rate of 250 points/s allowed 125 Hz as the highest frequency). The rectified EMG was averaged in each stage in each subject to quantify the level of activation in each muscle. A group average was then determined. The force was quantified in a similar manner by computing the mean force in each stage in each subject and then calculating the group mean in each stage. In addition, force variation in each stage was evaluated by determining standard deviation (SD) of the mean relative force.

2.2.4 Statistical Analysis

A repeated-measures general linear model was adopted for coherence comparisons between the stages and among the areas and muscles using SPSS 12.0 (SPSS Inc., Chicago, IL, USA). General linear model is a flexible generalization of ordinary least squares regression that incorporates a number of different statistical models: ANOVA, ANCOVA, MANOVA, MANCOVA, ordinary linear regression, t-test and F-test. In addition to analyzing amplitude of the coherence that above the significance level (95% confidence), the number of frequency bins reached the significance level was also quantified and analyzed. Since the frequency resolution was about 1 Hz, each 1-Hz step from 15 to 35 Hz consisted of one bin. The Z-transformed EEG power and normalized EMG power at beta band were also subjected to the analysis of the repeated-measures general linear model. The elbow flexion force, force variation (SD), and EMG of the relevant muscles were compared between stages 1 and 2 using paired *t* tests.

2.3 Results

The force and EMG results in the two stages of the sustained elbow flexion contraction were plotted as shown on Fig 2.3. Force was well maintained at about 30% maximal level (stage 1, 31.1% ± 2.45%; stage 2, 31.3% ± 2.43%). There was no significant difference in the force between stages 1 and 2 ($P > 0.05$). However, force variation (SD) in stage 2 (1.19 ± 0.27%) was greater than in stage 1 (0.80 ± 0.13%) ($P < 0.05$), indicating that although the mean force did not change, the force was less steady in stage 2 (Fig. 2.2A). Surface EMG signals of both the agonist (BB, BR) muscles increased significantly from less than 30% to near 40% maximal level ($P < 0.01$, Fig. 2.2B). The increase of the EMG of the elbow flexor muscles in stage 2 indicated that subjects had to increase their effort to maintain the same force, which was an indication of fatigue.

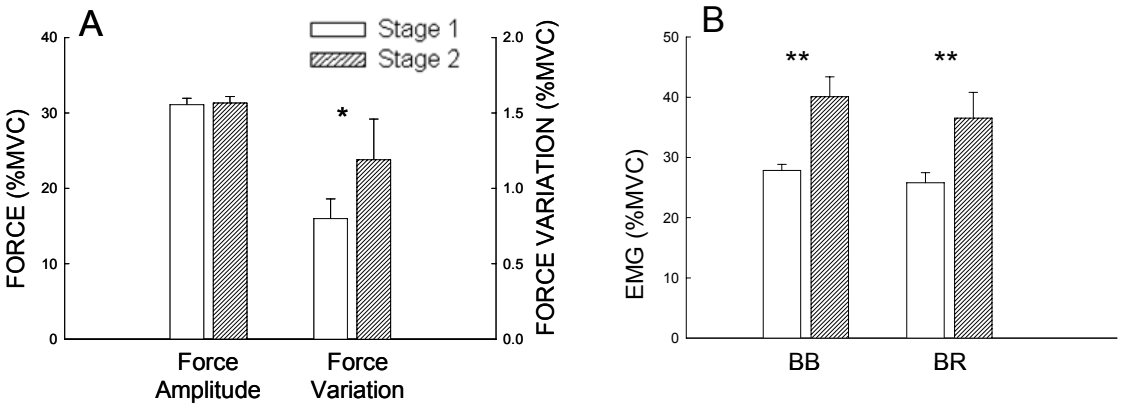

Fig. 2.3. Group averages of sustained force amplitude and variation (A), and surface EMG (B) for the two stages. Force and EMG were normalized to the maximal voluntary contraction (MVC) level. Force was maintained at the target level (30% MVC) for both stages, but the force became more variable or less steady in stage 2. The EMG level increased significantly in the fatigue stage (stage 2) for the two muscles. BB, biceps brachii; BR, brachioradialis. *$P \leq 0.05$; **$P \leq 0.01$.

EEG-EMG coherence decreased significantly in stage 2 compared with stage 1 at the beta band. A typical example of EEG (left scalp area)-EMG (BR muscle) coherence spectrum for one subject is shown in Fig 2.4A. This subject showed substantially reduced EEG-EMG coherence in stage 2 in left scalp area with all the muscles at the beta band. The subject exhibited significant coherence peaks within the beta band in stage 1. In stage 2, however, the coherence peaks either decreased or disappeared almost entirely. In contrast, the power of both the EEG and EMG signals increased at beta band in stage 2 (Fig. 2.4B, 2.4C).

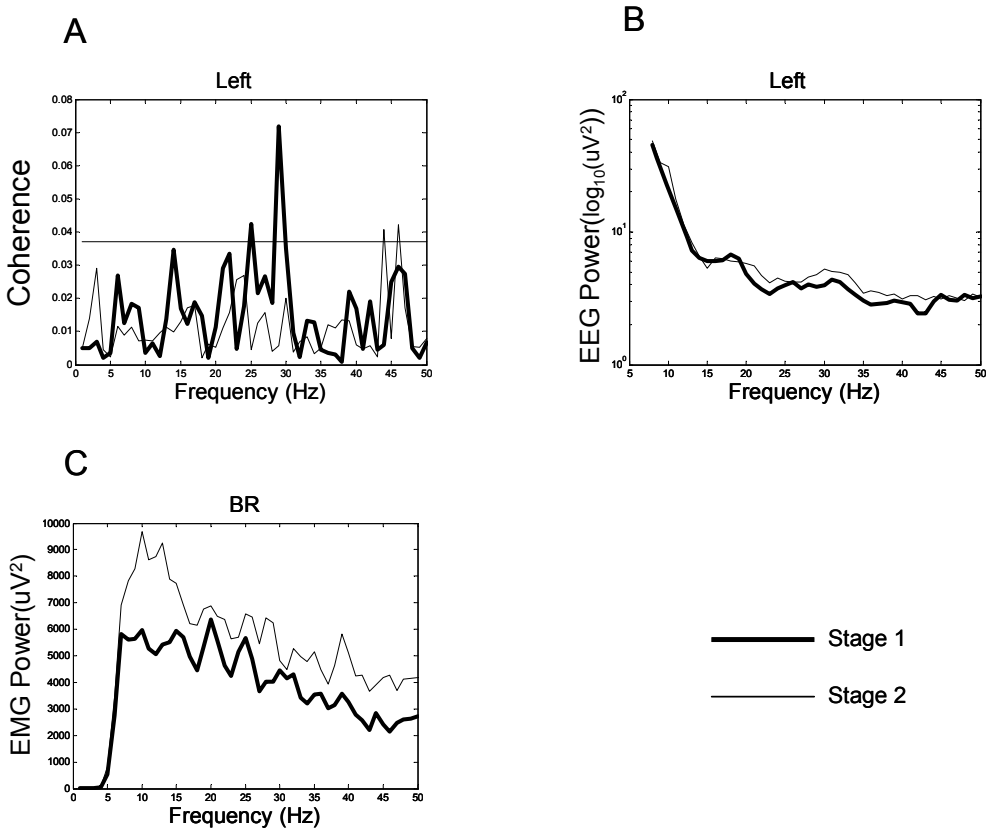

Fig. 2.4. A single-subject example of EEG-EMG coherence spectra between EEG of the left area and EMG of the brachioradialis (BR) muscle (A), EEG power spectrum of the left area (B), and EMG power spectrum of the BR muscle (C) in the two stages. On the coherence spectrum (A), a significant coherence peak at 30 Hz is clearly seen in stage 1 (thick line). In stage 2, however, the significant coherence peak disappeared (thin line). The horizontal line in A indicates 95% confidence level. The EEG power increased in stage 2 (thin line), especially in beta band (B). The EMG power elevated on the entire analyzed spectrum (C) in stage 2 (thin line).

Figure 2.5 displays coherence maps (average of the 9 subjects) based on electrodes within the five selected scalp areas with EMG of the three muscles for stage 1 (left column) and stage 2 (right column) at the beta band (15-35 Hz). Only significant coherence values were counted for each subject. The color bar indicates color-coded Z-transformed coherence values. The figure shows clearly that the level of coherence declined substantially in the fatigued compared to less-fatigued stage. The strongest coherence was located in the central-left-parietal areas in stage 1, especially for the two elbow flexor muscles (BB and BR). However, the spatial distribution of the coherence on the scalp with all the muscles altered dramatically in stage 2 with a majority of EEG channels showing weaker coherence and shifted scalp areas demonstrating strongest coherence (e.g., strong EEG-BB EMG coherence shifted from central-left [stage 1] to central-right [stage 2]; Fig. 2.5, top row).

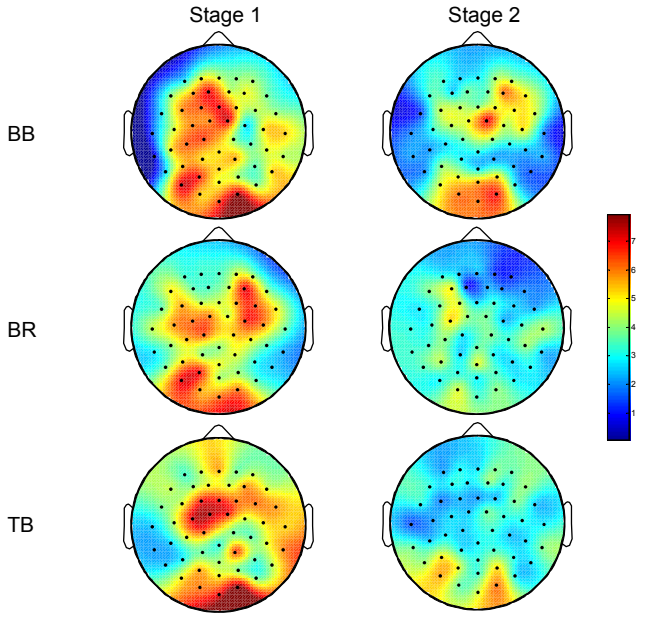

Fig. 2.5. Mapping EEG-EMG coherence based on coherence values of electrodes within the five selected scalp areas with EMG of the three muscles at beta (15-35 Hz) band in 9 subjects. The color bar indicates Z-transformed coherence values. The level of coherence declined substantially in stage 2 (fatigue condition, right column) compared with stage 1 (left column).

Statistical analysis of significant coherence values and bin numbers by a general linear model of repeated measures showed significantly lower corticomuscular coherence for stage 2 compared with stage 1 at beta band. No significant area-muscle-stage interaction was observed on the coherence measure, indicating the fatigue-related reduction in the coherence was a uniform phenomenon across scalp areas and muscles. The top row in Fig. 2.6 shows the number of frequency bins within the beta band (15-35 Hz) exhibited significant EEG-EMG coherence for all the scalp areas and muscles. Each displayed bin number for a given area-muscle combination in a given stage (e.g., left [L] area EEG with BB muscle EMG in stage 1) was derived by averaging the numbers across the EEG electrodes in a (e.g., left) scalp area with EMG of a muscle (e.g., BB) in a contraction stage (e.g., stage 1) in each subject first and then across the 9 subjects. The number of significant coherence bins within beta band was significantly smaller in stage 2 compared with stage 1 in all area-muscle combinations. Note that the bin number in Fig. 2.6 (upper row) was relatively small; this was primarily a result of spatial smoothing. For example, if one electrode was found to have 4 significant coherence bins in beta band in the left area (10 electrodes in each area), then the significant coherence bin number in this area would be only 0.25 (4 bins/10 electrodes). For the Z-transformed amplitude of the coherence, the value was also significantly lower in stage 2 vs. stage 1 for all the scalp area-muscle combinations (Fig. 2.6, bottom row).

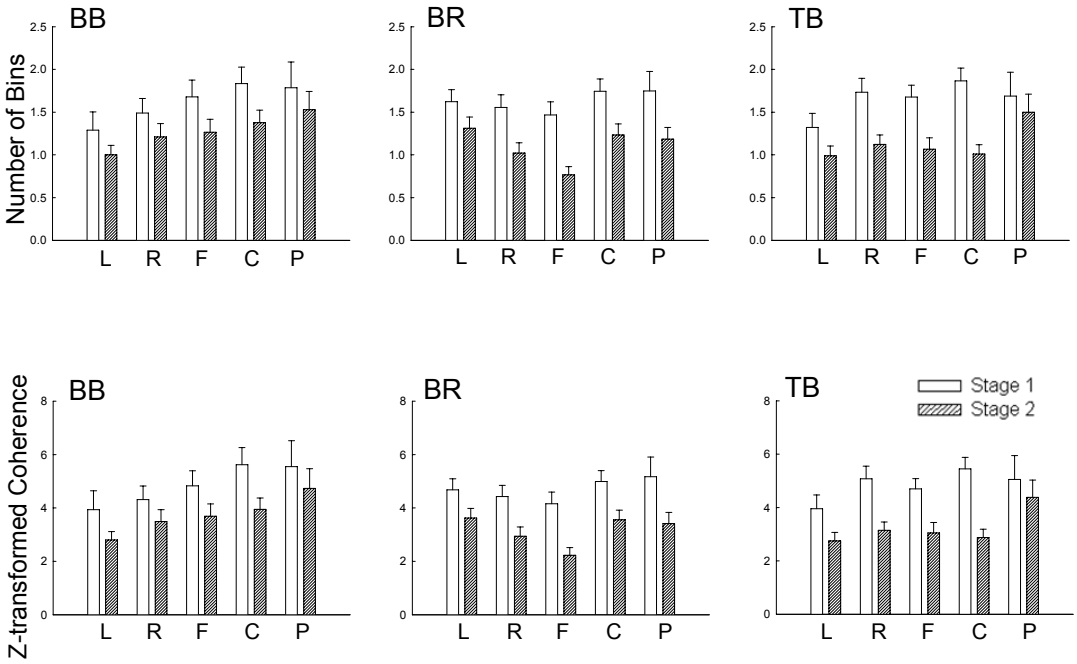

Fig. 2.6. Comparisons of the number of frequency bins with significant EEG-EMG coherence (upper row) and Z-transformed EEG-EMG coherence amplitude (lower row) between stages 1 and 2 among the five scalp areas and three muscles at beta frequency band. The data were based on results of nine subjects. Both the number of bins and the coherence amplitude significantly decreased with muscle fatigue ($P < 0.01$). Because there was no significant stage-area-muscle interaction, no post-hoc pair-wise comparisons were performed. BB, biceps brachii; BR, brachioradialis; TB, triceps brachii; L, left area; R, right area; F, frontal area; C, central area; P, parietal area.

Figure 2.7 shows results of the mean normalized EEG (Fig. 2.7A) and EMG (Fig. 2.7B) power at beta frequency band in stages 1 and 2. The EEG power increased in every scalp area. Statistical analysis of the EEG power revealed significant differences (P<0.01) between stages 1 and 2 and significant area effect. The normalized EEG power in the left and right areas was greater than that in the central, frontal and parietal areas. The EMG power was also increased in each muscle. Statistical analysis of EMG power by the general linear model showed a significant difference between stages 1 and 2 (P<0.01). No significant muscle and muscle-stage interaction on the EMG power was detected.

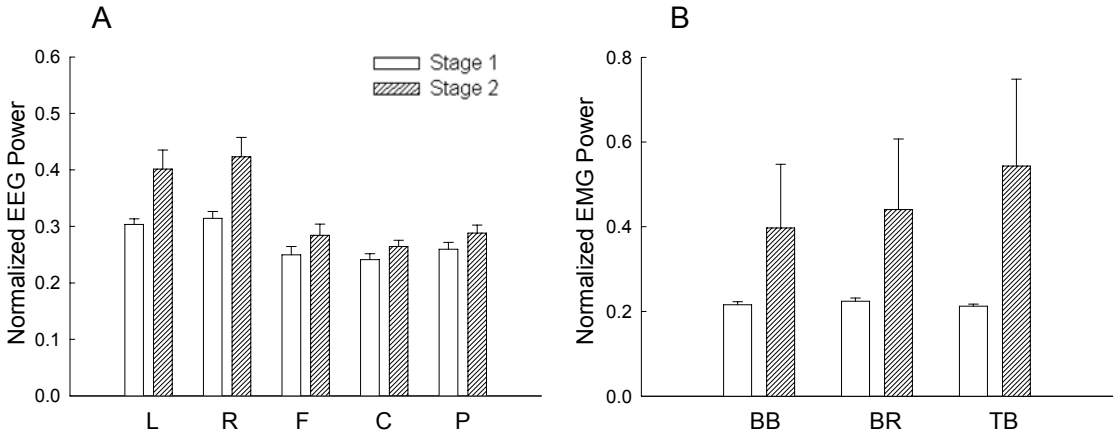

Fig. 2.7. Comparisons of the mean normalized EEG power of the five scalp areas and EMG power of the three muscles at beta band (15-35Hz) between stages 1 and 2. Data were based on results of nine subjects. Each normalized EEG power value in each area in each subject was an average of the values from all the electrodes in that area at beta band normalized to the total EEG power (3-50 Hz) in stage 1 of the same area. Similarly, the EMG power at beta band for each muscle was normalized to the total EMG power (10-125 Hz) in stage 1 of the same muscle. Both the EEG and EMG power increased with muscle fatigue ($P < 0.01$). Because there were no significant stage-area (EEG) and stage-muscle (EMG) interactions, no post-hoc pair-wise comparisons were performed. BB, biceps brachii; BR, brachioradialis; TB, triceps brachii; L, left area; R, right area; F, frontal area; C, central area; P, parietal area.

2.4 Discussion

Muscle fatigue involving voluntary motor activities is associated with acute adaptations in both the central nervous and muscular systems (Liu et al. 2003, 2005a and b, 2007; Post et al. 2007; van Duinen et al. 2007). Whether fatigue influences the strength of functional coupling between signals of the two systems is unknown. This study examined muscle fatigue effect on the level of corticomuscular coupling by computing the EEG-EMG coherence during a sustained voluntary submaximal elbow flexion. The major findings were that the EEG-EMG coherence decreased significantly from a stage of minimal fatigue to a stage of more severe fatigue.

Force, EMG and Fatigue

Fatigue-related changes in muscle force and EMG signals during maximal and submaximal muscle contractions have been studied extensively (Bigland-Ritchie, 1981, Enoka and Stuart, 1992). In a submaximal muscle contraction, in which a target force is sustained for a prolonged time, a major index of fatigue is amplitude of the EMG that increases with the level of fatigue (Liu et al., 2003, van Duinen et al., 2007). As a muscle fatigues, its ability to generate force declines (Gandevia, 2001); under this condition, additional motor units need to be recruited and/or the active motor units are driven to higher activation levels (reflected by augmented EMG) to maintain the same submaximal force. In this study, the EMG level of both the BB and BR, two major elbow flexors, increased significantly during stage 2 compared to stage 1 with maintenance of the target force across the two stages, indicating substantial muscle fatigue in stage 2.

Coherence Decreases in Fatigue Stage

The reduced EEG-EMG coherence during muscle fatigue suggests a fatigue-related weakening of functional coupling between cortical and muscular signals. There is general agreement that beta band coupling between the cortex and muscle is related to motor behavior (Conway et al., 1995, Kilner et al., 1999, Feige et al., 2000, Kilner et al., 2000, Kristeva et al., 2007). The coherence strength at the beta band has been demonstrated by systematic changes with motor parameters (Kilner et al., 2000). It has been further suggested that submaximal, low-level voluntary contractions are associated with corticomuscular signal coherence at the beta (15~30 Hz) frequency band (Conway et al., 1995), whereas strong voluntary contractions are associated with coherence at higher frequencies (30~60 Hz) (Brown et al., 1997). This beta band coherence observation

indicates perhaps a diminishing communication between the cortical output centers and muscles that received the cortical signals to carry out the intended motor action with increasing muscle fatigue. A number of mechanisms may contribute to the weakened coupling. One likely candidate is inhibitory drive from various sources that act upon the spinal alpha motor neurons. A number of studies applied transcranial magnetic stimulation over human motor cortex during sustained maximal or submaximal contractions demonstrated reduced excitatory input from the motor cortex to fatiguing muscle (Taylor and Gandevia, 2001, Sogaard et al., 2006). This lessening of descending drive has been interpreted as influences by inhibitory interneurons and/or the firing of fatigue-sensitive muscle afferents that act upon the corticospinal neurons and inhibit voluntary descending drive (Bigland-Ritchie, 1981, Leonard et al., 1994, Belhaj-Saif et al., 1996, Taylor et al., 2006). If the spinal and/or cortical output neurons are inhibited with muscle fatigue, their signals may not be as closely coupled with muscle activities as in the situation when muscle is less fatigued.

Impairments of neuromuscular junction (NMJ) transmission by fatigue may also contribute to the weakening of corticomuscular coupling. NMJ transmission function has been found to be reduced after muscle fatigue induced by sustained maximal (Bellemare and Garzaniti, 1988), submaximal (Fuglevand et al., 1993, Fuglevand et al., 1995), and electrical stimulation-evoked (Tanino et al., 2003) muscle contractions. NMJ transmission impairment is most significant following low-intensity sustained contractions (such as 30% maximal level used in this study) that lead to exhaustion (Fuglevand et al., 1993). If the descending command cannot be efficiently transmitted

from the brain to muscle across the NMJ under the condition of muscle fatigue, it is expected that the signal coupling between the brain and muscle would be affected.

Another potential contribution to the weakened corticomuscular signal coupling with fatigue is shifting of the cortical output center during prolonged motor activities. A recent study reported that as unilateral muscle fatigue became more severe, the center of brain activation shifted to locations more toward frontal, inferior, and ipsilateral directions (Liu et al., 2007). This observation was interpreted as "rotations" of cortical centers; as neurons in the original center became fatigued and reduced their activity, those in the other center(s) took over the function and maintained the overall level of brain-to-muscle drive (Liu et al., 2007). The coherence maps in Fig. 2.5 seem to support the "rotation" hypothesis. For example, the center of the peak coherence with BB muscle was in the central-left area in stage 1 but it shifted to the central-right area in stage 2 (Fig. 2.5, top row). The beta band EEG power in the right scalp area in Fig. 2.7A showed the largest increase compared to other scalp areas, indicating perhaps augmented activation in the ipsilateral sensorimotor regions. Under normal circumstances, voluntary muscle contractions are controlled by the primary motor cortex contralateral to the performing limb through the direct, monosynaptic corticospinal pathway. However, as the major control center is shifted to other locations with more indirect, polysynaptic pathways to the muscles, it is expected that the signals from the new centers would less tightly couple with the muscle signals.

Finally, fatigue-related motor unit firing behavior may also contribute to the weakened EEG-EMG coherence. It is a common observation that a person's hand/arm shakes (tremor at ~10 Hz) when he/she is severely fatigued (Ebenbichler et al., 2000).

The tremor could be a result of motor unit synchronization under fatigue condition. However, the increase in motor unit firing synchrony tends to have an effect in lower frequency bands (Arihara and Sakamoto, 1999) rather than the beta band (15-35 Hz), especially after applying the Discrete Fourier transform with hamming window for the calculation of the power spectrum and coherence. The application of hamming window reduces potential leakage or overflow of effects of a given frequency band to the adjacent frequency bins by suppressing the side lobes.

The change of EEG-EMG coherence could be influenced by increased EMG signals from muscles in or near the head areas under the fatigue condition. The increased EMG in the head area could easily contribute to the EEG signals and eventually affect the EEG-EMG coherence. Although this possibility could not totally be excluded, the chance of its occurrence was very low for the following reasons. First, before the data analysis, all the signals, especially the EEG signals were visually inspected and segments with visually-detected artifacts (e.g., EMG contaminations caused by eye blinks, jaw clenching, or tensing facial/neck/shoulder muscles) were discarded. Second, additional experiments were performed to further examine whether EEG with influence of EMG has an effect on EEG-EMG coherence. Two subjects performed two 2-min sustained elbow flexion contractions at 30% maximal level with the EEG (128 channels) and EMG of the elbow flexor muscles recorded simultaneously. In one contraction, they concentrated on the motor task without activating muscles in facial, neck, shoulder and other areas; in the other, they performed the task while slightly clenched the jaw so that the EEG signals were contaminated by EMG of the jaw closing muscles in the face. The analysis revealed that the power amplitude of the EMG-contaminated EEG had a sharp increase in the

gamma band (36-50Hz) compared with the power signal of the clean EEG. This increase of gamma power was not seen in the stage-2 EEG in the nine subjects in this study. More importantly, the EEG-EMG coherence was not different between the two conditions (EEG contaminated by jaw-clenching EMG and clean EEG) or even increased in the two subjects. These findings suggest that even if our stage-2 EEG data were contaminated by EMG of the near-by muscles after fatigue set in, the contamination did not affect the EEG-EMG coherence at the beta band.

EEG and EMG Power Increases in Fatigue Stage

It is worth noting that reduced corticomuscular coherence does not necessarily accompany a decrease in brain or muscle activation level. Tecchio et al. (2006) suggest that cortical recruitment and corticomuscular coupling are distinct mechanisms. During a sustained submaximal muscle contraction, both muscle (Fuglevand et al., 1993, Yue et al., 1997) and brain (Fuglevand et al., 1993, Liu et al., 2003, van Duinen et al., 2007) activation levels increase as fatigue sets in. The increased brain and muscle activities are thought to be a reflection of increasing descending command that result in recruitment of additional motor units and/or increasing activity level of the active motor units to compensate for the force loss contributed by those motor units that were recruited early but became fatigued (Liu et al., 2003, van Duinen et al., 2007). The result of the EEG and EMG power change in this study (Figure 2.7) was in line with the previous study. The mean EEG power at beta band significantly increased in stage 2 vs. stage 1, especially in the left and right scalp areas. These scalp areas overlie the major sensorimotor regions (i.e., contralatral and ipsilateral sensorimotor cortices that play an important role in controling voluntary muscle actions). The mean EMG power in the beta

band also significantly increased for all the muscles. The negative relation between the strength of corticomuscular signal coupling and amplitude of the signals during muscle fatigue suggests that the weakened neuromuscular coupling might be a tradeoff of increasing activation level to compensate for muscle fatigue. Weakened coupling could lead to lowering of quality in motor performance, such as increased force variation or reduced force steadiness observed with greater muscle fatigue (stage 2) in this study. The negative relation also underscores the likelihood of shifting the control centers during voluntary muscle fatigue as centers with less direct pathways to the muscle could enhance the level of muscle activation but lessen their functional coupling.

Summary

This study is the first to report significant weakening of functional corticomuscular coupling during muscle fatigue, which was demonstrated by large reductions in the level of EEG-EMG coherence. The weakening could be contributed by fatigue-related increases in inhibitory drive to the output centers, a decrease in neuromuscular junction transmission function, and shifting of primary output centers in the brain. The weakened coupling could be a potential cause of poor motor performance under fatigue condition. In the following chapter the fCMC change during the same muscle fatigue task in patients with cancer-related fatigue was investigated and compared to normal fCMC alterations exhibited by the healthy controls.

CHAPTER III

CANCER RELATED FATIGUE: FUNCTIONAL CORTICOMUSCULAR COUPLING IS WEAKENED

3.1 Introduction

Different from conventional muscle fatigue or fatigue in healthy individuals, cancer-related fatigue (CRF) is a persistent subjective sense of tiredness that interferes with daily activities (Mock et al., 2000). It comes on suddenly, does not result from activity or exertion, and is not relieved by rest or sleep. It might continue even after treatment is complete. CRF is widely recognized as the most common symptom and side effects of cancer and/or its treatment that exists in 25% to 99% of people with cancer, particularly in individuals actively undergoing treatment (Irvine et al., 1991, Donnelly and Walsh, 1995, Walsh et al., 2000, Cella et al., 2002, Servaes et al., 2002, Morrow et

al., 2005, Sood and Moynihan, 2005). However, research regarding understanding of physiological factors contributing to CRF is very limited.

Almost all previous studies that investigated fatigue in cancer patients relied on patients' responses to questionnaires (self report [SR] rating) to determine whether patients suffered CRF. Thus, although there are many instruments available to evaluate CRF, all have some limitations, and no single standard instrument exists for assessing overall CRF (review: Wu and McSweeney, 2001). No single instrument has been shown to correlate with a neurophysiological marker reflecting worsened feeling of fatigue in CRF. In fact, such biological/physiological markers of CRF have not been identified. And no single study has addressed the CRF with neurophysiological methods. Based on the definition that CRF is "an unusual persistent subjective sense of tiredness related to cancer or cancer treatment…," it is reasonable and logical to postulate that CRF involves malfunction of the brain, which can be investigated using modern neuroimaging (e.g., functional magnetic resonance imaging (fMRI)) and/or electrophysiological methods (e.g., electroencephalography (EEG)). Furthermore, CRF has been suggested to be related to neuromuscular abnormalities (Sood and Moynihan, 2005). Thus, fatigue assessments and studies by methods that could lead to clearer identifications of potential brain and muscle system mechanisms of CRF are needed.

Recently accumulating evidence suggests dissociation of muscle and supraspinal level system change during normal muscle fatigue (Gandevia et al., 1996, Butler et al., 2003, Liu et al., 2003, Liu et al., 2005, Liu et al., 2005). This weakening of brain-muscle coupling has been directly evaluated and reported in healthy subjects in Chapter 2 of this document. Given that there is a larger discrepancy between central and peripheral fatigue

and greater impairment in neuromuscular junction transmission function in CRF than controls (Yavuzsen T. et al., submitted), we have reason to believe that corticomuscular coupling is weakened in CRF, which could be the results of potential pathophysiological impairment. Distinguishing the cortical muscular functional couplings pattern in CRF patients with healthy controls would help to better understand the CRF mechanisms from neuromuscular perspective and contribute to identification of neurophysiological markers of CRF.

The present study was aimed at assessing potential muscle fatigue-related EEG-EMG coherence and power spectrum during sustained sub-maximal contractions of the elbow flexor muscles in CRF patients compared to healthy controls. We hypothesized that the level of fCMC (EEG-EMG coherence) in CRF patients would be lower than that in healthy controls due to the weakening of corticomuscular binding caused by pathophysiological impairment in the patient population.

3.2 Methods

3.2.1 Subjects

Eight cancer patients (62.9±12.3 years old, 5 men) and nine healthy subjects (48.2 ±14.8 years old, 3 men) participated in the study. No patients received chemotherapy or radiation therapy within four weeks prior to the study and all had to be postoperative for at least 4 weeks. Eligible patients had a hemoglobin concentration >10 g/dl, and no clinical evidence of polyneuropathy, amyotrophy, or a myasthenic syndrome by history and physical examination. Significant pulmonary compromise as determined by oxygen dependence was an exclusion criterion for both groups. Patients and controls who were

depressed or currently on psychostimulants or antidepressants were excluded. A single question "are you depressed" was used to exclude significant depression. Patients with weight loss greater than 10% of pre-illness body weight were excluded. The study was approved by Institutional Review Board at the Cleveland Clinic. All subjects gave informed consent prior to their participation. All subjects performed a sustained contraction of the right-arm elbow flexion at 30% maximal level until subjective exhaustion. Elbow flexion force, surface EMG and multi-channel EEG were simultaneously recorded during the sustained contraction.

3.2.2 Data Recording

Please refer to Chapter 2 Data Recording section for details

3.2.3 Data Processing and Analysis

During offline processing, the EEG signals were re-referenced to the average value of all 128-channel signals (exclude the outmost electrodes) and high-pass filtered at 3 Hz; the EMG signals were resampled at 250 Hz and high-pass filtered at 10 Hz to minimize low-frequency baseline fluctuation before rectification. All signals, especially the EEG were inspected visually. Recordings with artifacts caused by events such as eye blinks or head movements were excluded and the corresponding EMG signals discarded. The entire duration of the EEG and EMG recordings was then divided into the first half (stage 1 with minimal fatigue) and second half (stage 2 with severer fatigue). And subsequently the signals in each stage were segmented into artifact-free epochs of 256 samples without overlapping (mean = 98.5 epochs, ranged from 44 to 153 for CRF and mean = 148.5 epochs, ranged from 56 to 264 for controls).

Due to the volume of information, especially the large number of EEG channels,

the coherence values of EEG channels overlying sensorimotor function-related brain regions with each of the three muscles (biceps brachii [BB], branchioradialis [BR] or triceps brachii [TB]) were grouped into five scalp areas for statistical comparisons (ten electrodes in each scalp area): left, right, frontal, central and parietal (see Fig. 2.2). Crossing-stage comparisons were limited to the beta (15-35Hz) frequency band since most of the significant EEG-EMG coherence values were only detected at the beta frequency band in both stages 1 and 2. The calculated coherence was Z-transformed by the arc hyperbolic tangent transformation to stabilize the standard deviation (Rosenberg et al., 1989). The transformation was as follows:

$$Z = \arctan h(\sqrt{C}) \times \sqrt{2L}$$

Where C is the coherence value and L is the number of epochs.

The coherence estimation method was the same as that described in the last chapter.

3.2.4 Statistical Analysis

A repeated measures general linear model was used to statistically compare the coherence between CRF patients and controls among different stages, muscles and areas with a covariate of age by SPSS 12.0 (SPSS Inc., Chicago, IL, USA). The EMG amplitude of CRF patients and controls were also compared using repeated measures general linear model.

3.3 Results

The elbow flexion force was well maintained at about 30% maximal level and there was no significant difference of force between stage 1 and stage 2 in the patient or

control group. The EMG results in the two stages of the sustained elbow flexion were plotted on Fig 3.1. The amplitude of surface EMG signals from the elbow flexor muscles (BB, TB) increased significantly (P<0.01) in both groups. The normalized EMG amplitude was not different either between the groups or muscles. The increase of the surface EMG of the involved elbow flexor muscles in stage 2 indicated that subjects had to increase their effort to maintain the same force level, which was an indication of fatigue.

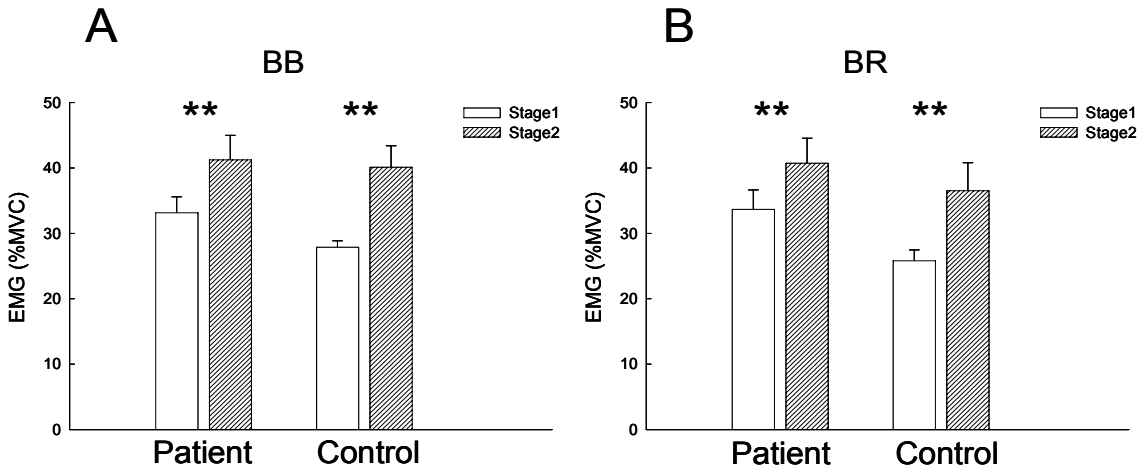

Fig. 3.1. The EMG amplitude of patients and controls in the two stages of the sustained elbow flexion for each agonist muscle. BB: biceps brachii, BR:brachioradialis

EEG-EMG coherence of CRF patients decreased significantly in stage 2 compared with stage 1 at the beta band. A typical example of EEG (left scalp area)-EMG (BB muscle) coherence spectrum for one subject is shown in Fig 3.2A. The subject exhibited significant coherence peaks within the beta band (15-35 Hz) in stage 1. In stage 2, however, the coherence peaks had an obvious reduction. In contrast, the power of both the EEG and EMG signals increased at beta band in stage 2 (Fig. 3.2B, 3.2C). This

coherence reduction in beta band was consistent with the results of the healthy controls (Fig. 3.2).

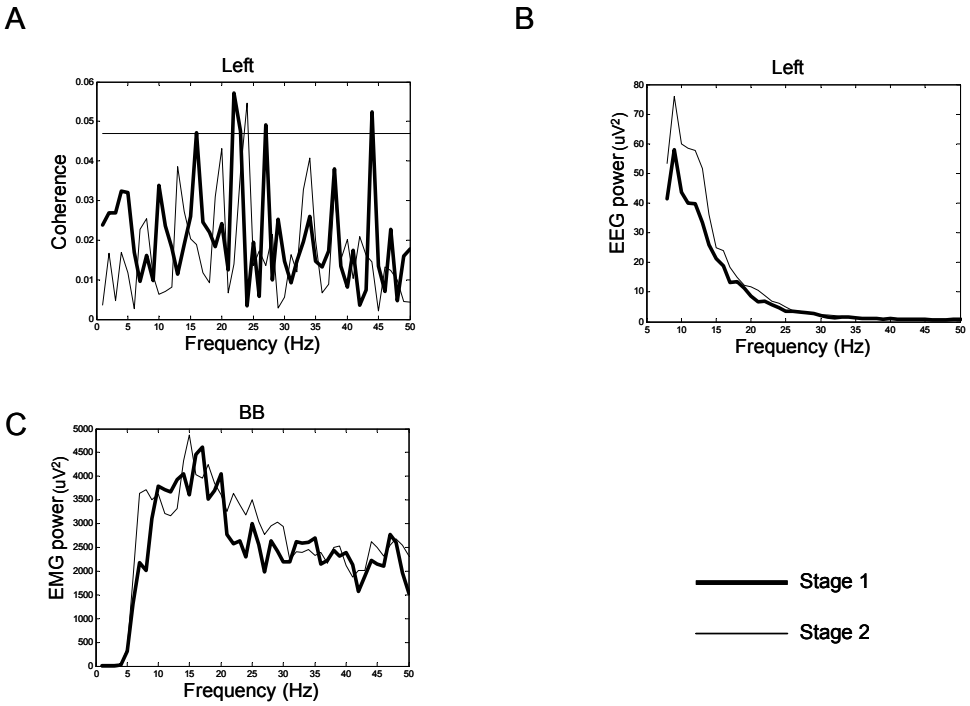

Fig 3.2. A single-subject example of EEG-EMG coherence spectra in CRF patients between EEG of the left area and EMG of the biceps brachii (BB) muscle (A), EEG power spectrum of the left area (B), and EMG power spectrum of the BB muscle (C) in the two stages. The horizontal line in A indicates 95% confidence level.

Figure 3.3 shows the number of frequency bins within beta band (15-35 Hz) exhibited significant EEG-EMG coherence for all the scalp areas and muscles of each group. Each displayed significant bin number for a given area-muscle combination in a given stage (e.g., left [L] area EEG with BB muscle EMG in stage 1) was derived by averaging the numbers across the EEG electrodes in a (e.g., left) scalp area with EMG of a muscle (e.g., BB) in a contraction stage (e.g., stage 1) in each subject first and then across the 9 subjects. The statistical analysis of coherence bin numbers showed significant group difference (P<0.01) with significant group-stage interaction (P<0.01). Subsequently, further comparison based on general linear model within each stage was

performed. In stage 1, the bin number in CRF patients was significantly smaller ($P<0.01$) than healthy controls and the number was not significantly different between the groups in stage 2. The statistical analysis also showed significant stage effect ($P<0.01$) with significant scalp area $\times$ stage interaction ($P<0.01$), which means the coherence was significantly reduced from stage 1 to stage 2 for both groups and the degree of reduction was significantly different among the areas. The coherence in the left scalp area of CRF patients obviously did not decrease substantially from stage 1 to stage 2. For the Z-transformed coherence amplitude, the statistical results were almost the same as the bins number of significant coherence, but the trends (Fig. 3.4) was clearer than that of the bins number (Fig. 3.3). The covariate age was not significant in any of these statistical analyses.

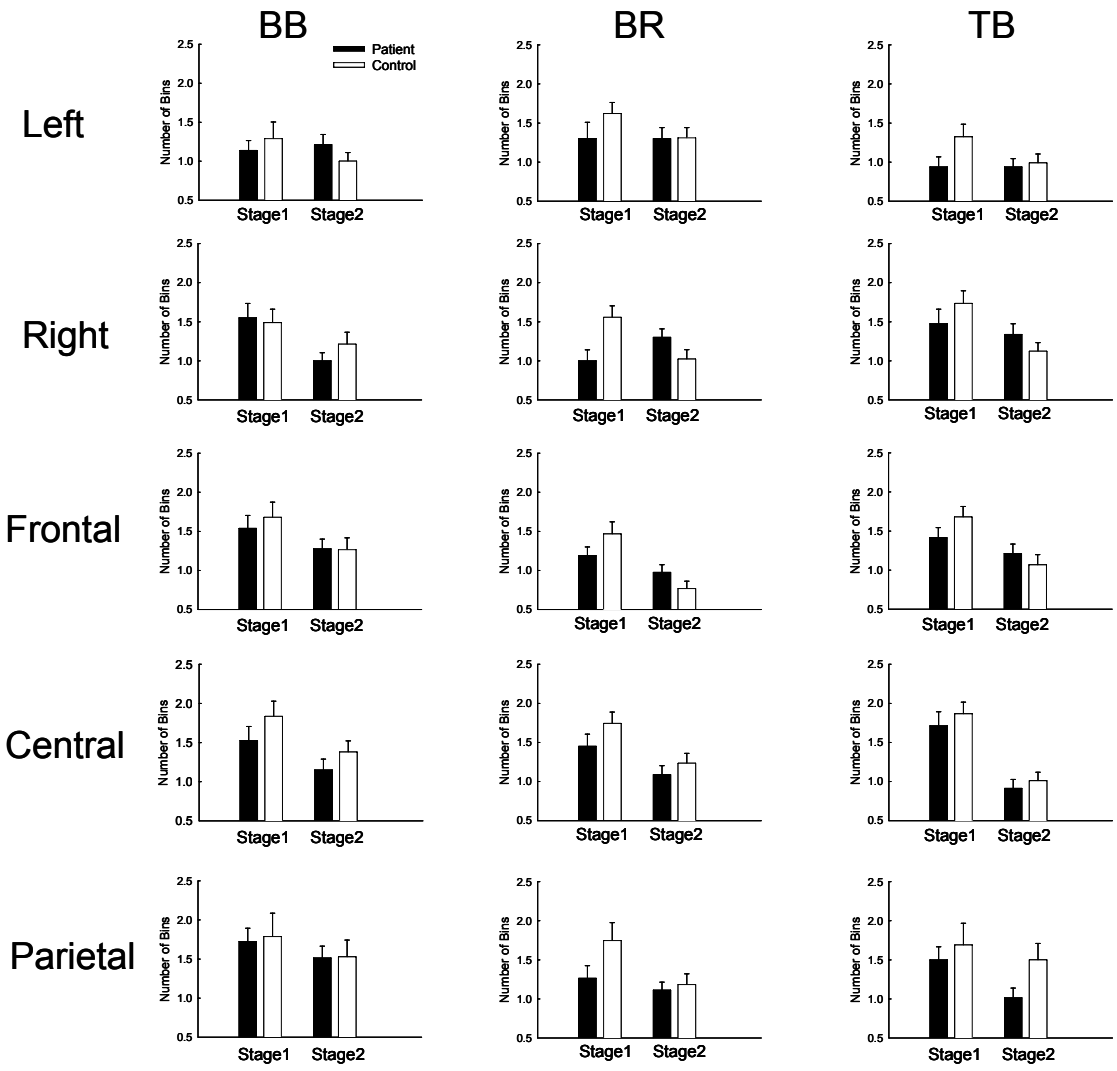

Fig 3.3. Comparisons of the number of frequency bins with significant EEG-EMG coherence between stages 1 and 2 among the five scalp areas and three muscles at beta frequency band. The data were based on results of eight CRF patients and nine controls. The number of bins in CRF patients was significantly lower compared to the controls ($P < 0.01$) and both group exhibited significantly decreased number of bins with muscle fatigue ($P < 0.01$). See details in Results. BB, biceps brachii; BR, brachioradialis; TB, triceps brachii.

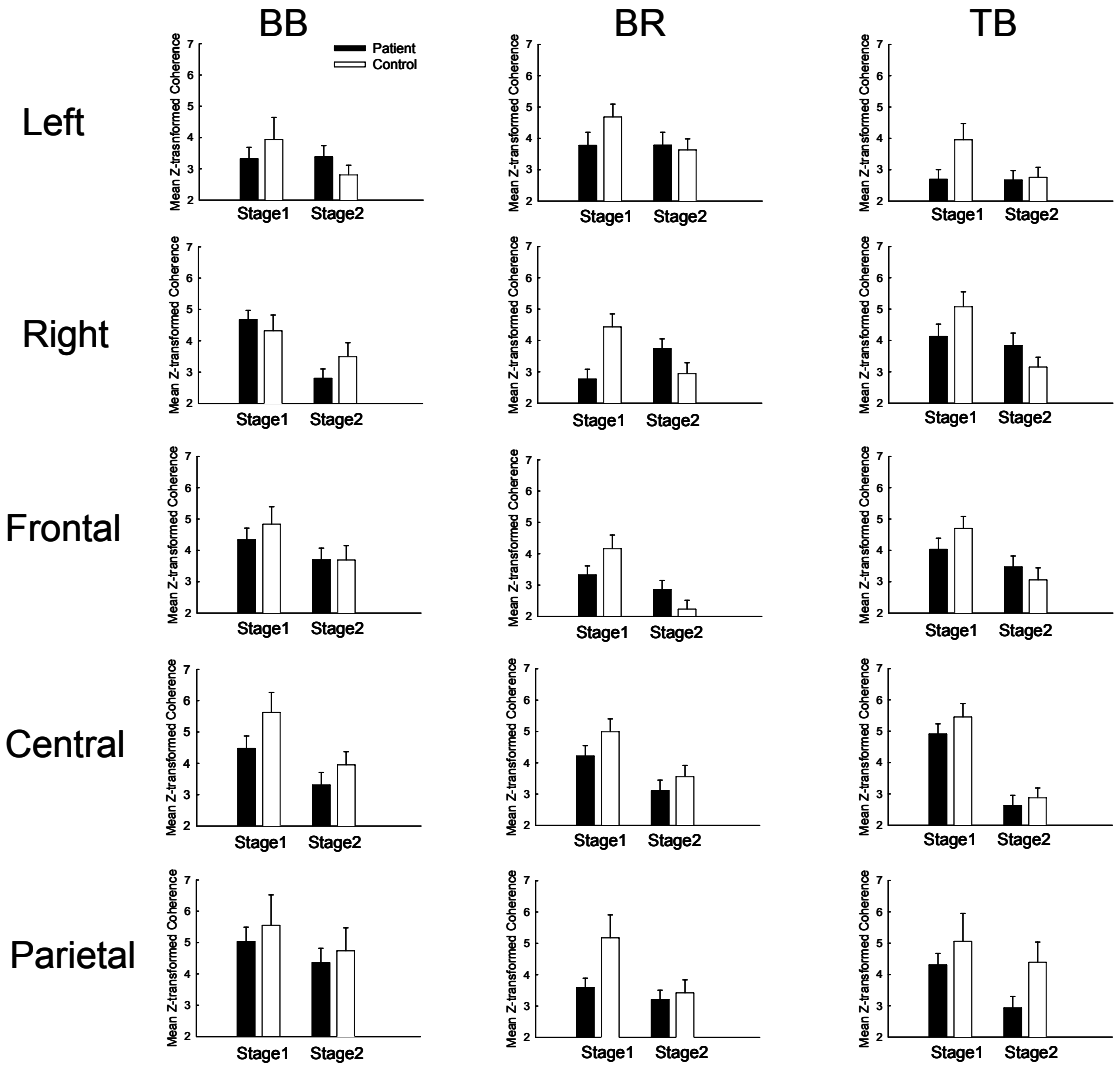

Fig. 3.4. Comparisons of the Z-transform significant EEG-EMG coherence values with between stages 1 and 2 among the five scalp areas and three muscles at beta frequency band. The data were based on results of eight CRF patients and nine controls. The coherence values in CRF patients was significantly lower compared to the controls ($P < 0.01$) and both group exhibited significantly decreased coherence values with muscle fatigue ($P < 0.01$). See details in Results. BB, biceps brachii; BR, brachioradialis; TB, triceps brachii; L, left area; R, right area; F, frontal area; C, central area; P, parietal area.

Figure 3.5 displays coherence maps (average across subjects in each group) based on the 128 EEG channels with EMG of the three muscles for stage 1 (first and third columns) and stage 2 (second and fourth columns) at the beta band (15-35 Hz) for CRF patients (first two columns) and controls (last two columns). Only significant coherence values were counted for each subject. The color bar indicates color-coded Z-transformed

coherence values. The figure shows clearly that the level of coherence declined substantially in the fatigued compared to less-fatigued stage and the overall level of coherence in CRF patients was higher than controls in stage 1. The strongest CRF coherence with BB and BR muscle was located in the left-parietal area in stage 1, which was more parietal compared to the spatial distribution map of controls. And in stage 2 the spatial distribution of the coherence on the scalp altered dramatically with a majority of EEG channels showing weaker coherence in both groups and shifted scalp areas demonstrating strongest coherence in control group (e.g., strong EEG-BB EMG coherence shifted from central-left [stage 1] to central-right [stage 2]; Fig. 3.5, top row of last column).

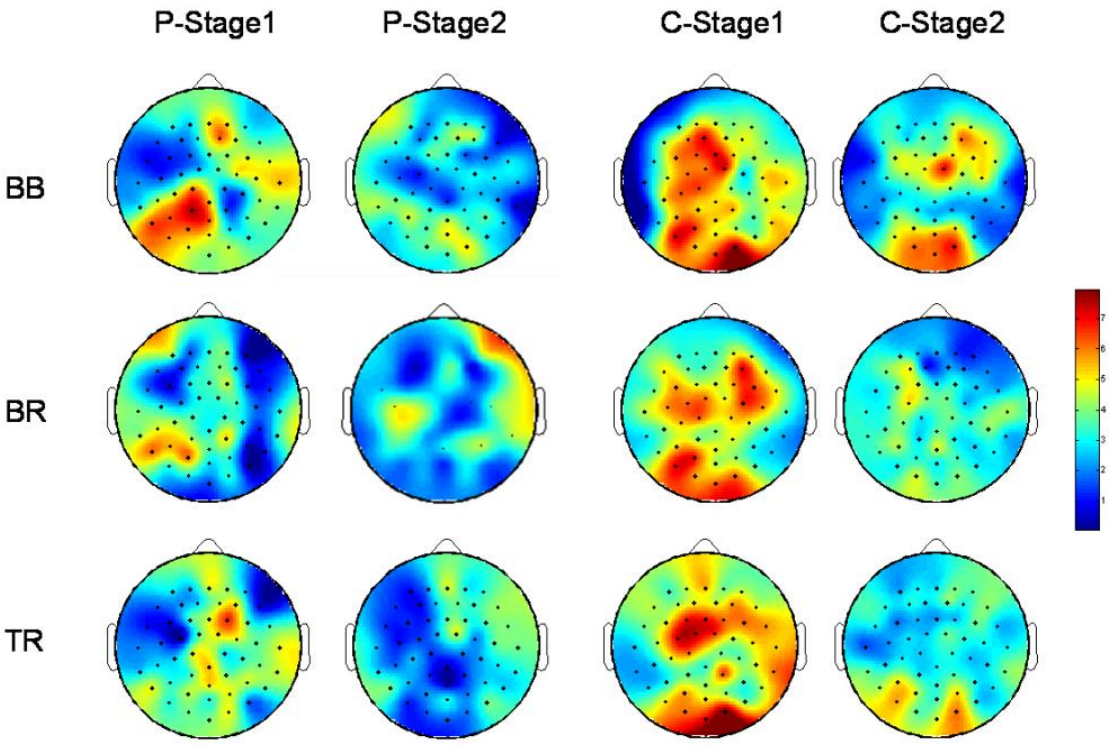

Fig.3.5. Mapping EEG-EMG coherence based on significant coherence values of the selected 128 EEG channels with EMG of the three muscles at beta (15-35 Hz) band in CRF patients (left two columns) and healthy subjects(right two columns). The color bar indicates Z-transformed coherence values. The level of coherence declined substantially in stage 2 (fatigue condition, 2nd and 4th

columns) compared with stage 1 (1st and 3rd columns). The coherence values in CRF patients were significantly lower compared to the controls.

Figure 3.6 shows results of the mean normalized EEG power at beta frequency band in stages 1 and 2. The EEG power was significantly larger in CRF patients in every scalp area (P<0.01). And each group showed a significant increase from stages 1 to stage 2 (P<0.01). Since the area factor was significant (P<0.01), further multiple comparisons between each area were performed. The left and right scalp areas were significantly different from other areas (P<0.05). No significant interactions were detected.

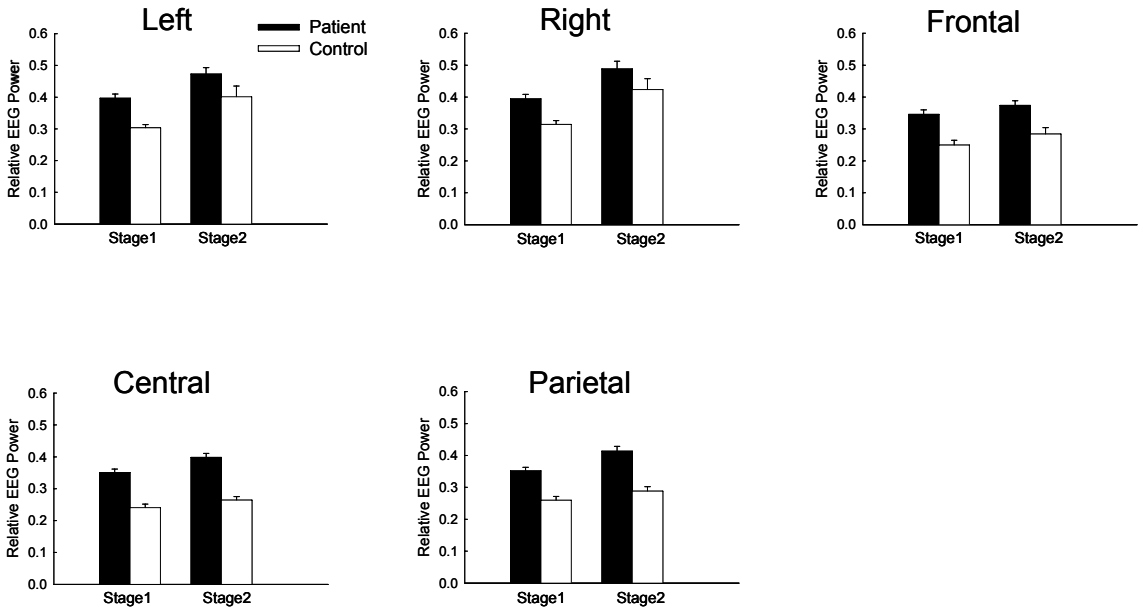

Fig.3.6. Comparisons of the mean normalized EEG power of the five scalp areas at beta band (15-35Hz) in stages 1 and 2 between the CRF patients and healthy controls. The data were based on results of eight CRF patients and nine controls. Each EEG normalized power value in each area in each subject was an average of all values from all the electrodes in that area at beta band normalized by first stage total power value. The EEG power increased with muscle fatigue (P < 0.01). And the CRF patients showed significant higher values of EEG power compared to the controls (P < 0.01). See details in Results. L, left area; R, right area; F, frontal area; C, central area; P, parietal area.

The mean normalized EMG power at beta frequency band was shown in Figure 3.7. Within each group there was a significant increase from stage 1 to stage 2. Statistical analysis of EMG power by the general linear model showed a significant difference

between stages 1 and 2 (P<0.01). But there was no significant difference between the CRF patients and healthy controls, although there was a trend that the EMG amplitude was lower in CRF patients compared to controls in the severe fatigue stage.

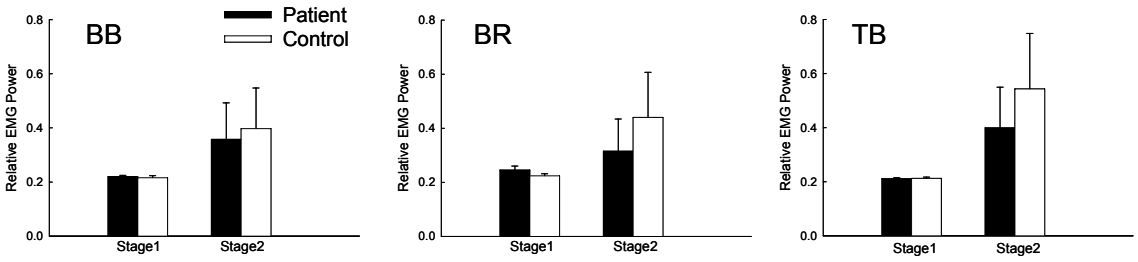

Fig.3.7. Comparisons of the mean normalized EMG power of the five scalp areas at beta band (15-35Hz) in stages 1 and 2 between the CRF patients and healthy controls. The data were based on results of eight CRF patients and nine controls. Each EMG normalized power value in each area in each subject was an average of all values from all the electrodes in that area at beta band normalized by first stage total power value. The EMG power increased with muscle fatigue (P < 0.01). See details in Results. BB, biceps brachii; BR, brachioradialis; TB, triceps brachii.

3.4 Discussion

This study, for the first time, showed that the level of EEG-EMG coherence was significantly lower for CRF patients compared to healthy controls within minimal fatigue stage despite the fact that the EEG power was higher in CRF patients. The coherence significantly decreased from minimal to more severe fatigue stages for both patient and control groups.

The novel finding that EEG-EMG coherence was significantly weaker in CRF patients in minimal fatigue stage suggests the weakened or impaired corticomuscular coupling in CRF patients. The voluntary muscle contraction activity is dependent on smooth and ordered flow of nerve impulses in major motor and sensory systems. The components in the whole process include cognitive processing, the generation of motor commands from the cortices, motor output from spinal cord, neuromuscular junction

(NMJ), muscle contraction and sensory feedback. Since EEG-EMG coherence value reflects the degree of the oscillatory activity binding between the central nervous system (CNS) and muscle (Kilner et al., 2000), impairment in any of the components or block of the link at any level during the process would increase the dissociation of the signals in the brain and muscle systems. The decrease in EEG-EMG coherence in CRF is a reflection of the dissociation. Several factors or mechanisms could contribute to the decreased EEG-EMG coherence. One likely candidate is defects in neuromuscular junction (NMJ) transmission, which has been suggested in the previous study in our laboratory (Yavuzsen et al. 2007). The M-wave amplitude was 50% lower in CRF than controls, both before and after muscle fatigue. The M-wave measures muscle response evoked by an electrical stimulus applied to the motor nerve proximal to the NMJ and the measurement was made on the muscle distal to the NMJ; thus, it is a gross assessment of efficiency of NMJ transmission. If the central signals can not be efficiently transmitted across the NMJ, muscle will not be fully recruited into contraction, which would possibly prevent muscle activation and weaken the binding between the CNS and muscle. In a similar manner NMJ propagation efficiency decreased and fatigue increased in prostate cancer patients undergoing radiation therapy which improved 5 to 6 weeks after radiation (Monga et al., 1997).

Another possible reason is the reduced central drive from cortex to muscle. Our previous study has suggested CRF is centrally-mediated fatigue. This was supported by the facts that CRF patients exhibited greater subjective fatigue (higher BFI score and feeling exhaustion sooner during the sustained muscle contraction) but physiological indices indicated they experienced less muscle fatigue at the end of the sustained

contraction. The current pathophysiological changes found in CRF patients may also explain the weakened binding of CNS and muscles, such as cytokine change, neuromuscular abnormalities and neuroendocrine changes (Sood and Moynihan, 2005). Among these factors, the increased pro-inflammatory cytokines in CRF patients may indicate the immune process is switched on by cancer or cancer treatment, which can signal the brain, leading to a variety of effects including fatigue (Bower, 2006). But exactly how and where these factors take effect is still unknown. It is unlikely that this coherence difference of CRF patients and controls was due to their age difference. The statistical analysis has shown the coherence value was not correlated with age. And none of the studies has shown fCMC was correlated with age.

The significant decrease of EEG-EMG coherence from non-fatigue to fatigue stage in patients was consistent with the coherence changes in healthy controls doing the same motor task. This decrease may be due to fatigue-related increases in inhibitory drive to the output centers (Bigland-Ritchie, 1981, Leonard et al., 1994, Belhaj-Saif et al., 1996, Taylor et al., 2006), a decrease in neuromuscular junction transmission function (Bellemare and Garzaniti, 1988, Fuglevand et al., 1993, Fuglevand et al., 1995), and shifting of primary output centers in the brain (see chapter 2 for details). All these changes are physiologically induced by a fatiguing motor task, which can be recovered by rest or sleep, while those changes that contribute to the lower coherence value in CRF patients compared to the controls in both stages of fatigue motor task may be mainly due to the pathophysiological reasons induced by cancer or cancer treatment, which may not be recovered just by rest (Chaudhuri and Behan, 2004, Sood and Moynihan, 2005).

It is interesting to see that the EEG-EMG coherence was not significantly different between the CRF patients and healthy controls in stage 2. That means the coherence value reduction from minimal fatigue to severe fatigue stage was less in CRF patients than that in healthy controls. As one can see from Figure 3.3 and Figure 3.4, the beta band coherence of the left scalp area EEG with all the muscles was not significantly different between two stages of the fatigue motor task in patient group compared to control group. This is understandable. The reduction of coherence from stage 1 to stage 2 was likely induced by muscle fatigue-related physiological changes in each group. Since the CRF patients experienced less muscle fatigue than controls when exhausted (Yavuzsen et al. submitted), less reduction of coherence value would be taken from the CRF patients. So in stage 1 due to pathophysiological impairment, CRF patients exhibited lower coherence value than controls. While in stage 2, less reduction of coherence value induced by physiological changes of muscle fatigue in CRF patients was balanced by the greater reduction of coherence resulted from pathophysiological conditions, leading to the insignificant coherence change in the patient group.

During a sustained submaximal muscle contraction, both muscle (Fuglevand et al., 1993, Yue et al., 1997) and brain (Fuglevand et al., 1993, Liu et al., 2003, van Duinen et al., 2007) activation levels increased as fatigue sets in. The increased brain and muscle activities are thought to be a reflection of increasing descending command that results in recruitment of additional motor units and/or increasing activity level of the active motor units to compensate for the force loss contributed by those motor units that were recruited early but became fatigued (Liu et al., 2003, van Duinen et al., 2007). The CRF EEG power was significantly increased from stage 1 to stage 2 in each scalp area to

compensate for the fatigue effect, which was the same as the EEG power changes in controls. But the EEG power in CRF patients throughout the fatigue motor task was significantly higher compared to the controls. This suggests that the CRF patients had to try harder to sustain the same level of relative force. The fact that the EMG power change was not significantly different between two groups indicates that the greater voluntary effort (greater EEG power) in CRF patients did not translate into higher muscle power. This phenomenon could be explained by the finding of reduced NMJ transmission function in CRF (part of brain signal is blocked by the NMJ).

In conclusion, this study uses objective neuromuscular index: the EEG-EMG coherence to directly evaluate the corticomuscular coupling in CRF patients. The results indicate significant weakening of corticomuscular coupling in CRF patients. Because CRF patients experienced less muscle fatigue during the sustained contraction, the level of corticomuscular coupling does not decline as much as healthy individuals at the times of more severe feeling of fatigue (e.g., stage 2). In Chapters II and III, EEG-EMG coherence was calculated by averaging many epochs of the EEG and EMG data, which yielded only two values: EEG-EMG coherence in stage 1 and the coherence in stage 2. This approach has apparent limitation of poor time resolution. In the following chapter, procedures and results of single-trial EEG-EMG coherence in a handgrip motor task were described.

CHAPTER IV

DETECTING FUNCTIONAL CORTICOMUSCULAR COUPLING DURING FATIGUE IN SINGLE TRIAL

4.1 Introduction

The experimental design used in the study of fatigue is either intermittent submaximal/maximal muscle contraction or sustained submaximal/maximal muscle contraction to exhaustion. The common practice in data analysis is to detect physiological and muscle output differences between the pre-fatigue and after-fatigue measurements (Tecchio et al., 2006) or compare block results after dividing the whole fatigue data into a number of blocks (Gandevia et al., 1996, Butler et al., 2003, Liu et al., 2005, Liu et al., 2005). However, different from other conditions, fatigue is a progressive process: the ability of a muscle to generate force declines progressively by time. It would be more interesting to see how fatigue progresses trial-by-trial in an intermittent-muscle-

contraction design or how fatigue is induced by time in a sustained muscle contraction. Compared with the traditional coherence estimation method used in chapter 2 and chapter 3, the single trial analysis can provide more detailed and useful information such as whether different subjects behave in the same trend in a trial-by-trial basis. Furthermore, the single trial analysis permits a real-time quote of the coherence and frequency power spectra.

Coherence is a tool to analyze the linear relationship between two signals in frequency domain using normalized cross-spectrum. The well-established coherence analysis based on fast Fourier Transform (FFT) does not allow an accurate estimate of coherence in single trial, because it smoothes the spectrum by averaging multiple trials. The FFT method assumes each trial has the same physiological activities repeated at the same latency, which is at least not applicable to all the cases and has not yet been validated. An alternative method is to smooth the spectrum across time based on the assumption of stationarity of the signal. When a signal is non-stationary as most of the physiological signals are, traditional Fourier analysis is not adequate. The time-frequency analysis where coherence can be estimated as a function of time is recommended for analyzing non-stationary signals. Although several successful attempts have been brought to adapt Fourier-based methods to shorter time signals (Lovett and Ropella, 1997, Xu et al., 1999, Perez et al., 2005), this project proposed to estimate EEG-EMG coherence of single trial based on time-frequency analysis of wavelet transform. Wavelet transform provides the optimal time and frequency concentration which makes it a good candidate to capture the rapidly changing spectra of non-stationary signals (Lachaux et al., 2002, Issartel et al., 2006, Klein et al., 2006).

This study proposed the single trial coherence estimation based on time-frequency wavelet analysis and applied this to investigate fatigue effect on the coherence trial by trial during repetitive maximal muscle contractions in eight healthy subjects. It was hypothesized that the EEG-EMG coherence and signal energy would decrease with muscle fatigue; each subject would show a unique dynamic pattern with time when more detailed information was revealed by single trial analysis.

4.2 Methods

4.2.1 Wavelet Coherence

The wavelet that has been used in neuroscience field (Tallon-Baudry et al., 1997) is the complex Morlet wavelets. Complex Morlet's wavelets have a Gaussian shape both in the time domain (SD σ_τ) and frequency domain (SD σ_f) around its central frequency f_0 :

$$w(\tau, f_0) = A\exp(-\tau^2 / 2\sigma_t^2)\exp(2i\pi f_0\tau) \tag{4.1}$$

$$\sigma_f = 1/2\pi\sigma_\tau \qquad f_0/\sigma_f = N_{co} \quad A = (\sigma_\tau\sqrt{\pi})^{-1/2} \tag{4.2}$$

N_{co} is the number of cycles of Morlet wavelets that determines the compromise between time and frequency. The wavelet transform of a signal is the result of the convolution of the complex wavelet with the signal and the time-varying energy of the signal in a frequency band is the square norm of the result of the wavelet transform.

The wavelet cross-spectrum between signal x and signal y around time t and frequency f can be defined from the wavelet transform (Wx(τ,f) and Wy(τ,f)) (Lachaux et al., 2002):

$$SW_{xy} = \int_{t-\delta/2}^{t+\delta/2} W_x(\tau, f) \cdot W_y{}^*(\tau, f) d\tau \tag{4.3}$$

* indicates the complex conjugate and δ is a scalar that depends on frequency.

Then the wavelet coherence Wco(t,f) at time t and f is defined as followings,

$$Wco(t, f) = \frac{\left| SW_{xy}(t, f) \right|^2}{SW_{xx}(t, f) \cdot SW_{yy}(t, f)} \tag{4.4}$$

This wavelet coherence estimate smoothes the power spectrum (auto-spectrum and cross-spectrum) across a short interval [t-δ/2, t+δ/2]. The difference between this wavelet coherence estimate and Fourier-based short time coherence estimate is that δ is constant for all frequencies in Fourier-based method, while δ varies with frequency in wavelet-based method. Lower δ values correspond to higher frequencies, which provide the advantage of being able to track the dynamically changing coherence. The δ is time resolution of the time-frequency wavelet coherence estimation. If the smooth cycle in the integration window [t-δ/2, t+δ/2] is defined as $N_{cy,}$ the δ can be determined as N_{cy}/f. So when using a window of integration of N_{cy} cycles at frequency f, the wavelet spectra are smoothed or averaged over the interval [t-δ/2, t+δ/2],

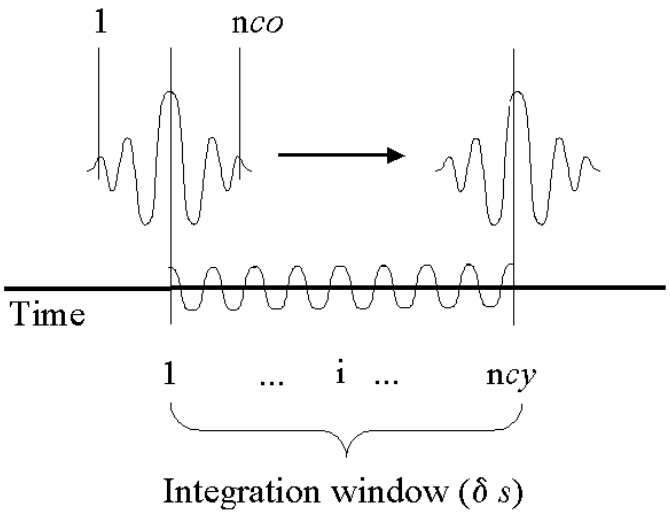

Fig.4.1. Definition of parameters N_{cy} and N_{co}. For each frequency, the wavelet coherence averages the wavelet coefficients over an interval of size δ that adapts to f. δ corresponds to a constant number of oscillations cycles: δ = N_{cy}/f. The wavelet-coefficients are computerd by convoluting the signals with successive N_{co} –cycle Morlet wavelets. Lachaux et al. Neurophysiol Clin 32: 157-174, 2002.

where $\delta = N_{cy}/f$. The wavelet spectra at t-δ/2 result from a segment of data in [t-δ/2-w/2, t-δ/2+w/2], where w is the width of the wavelet at frequency f, $w = N_{co}/f$ (please refer to Fig. 4.1). The total data window needed for each wavelet coherence value calculation at frequency f is $\delta+w = (N_{cy+} N_{co}) / f$ (Fig. 4.1).

The significance level was obtained from an average of 100 pairs of independent random white-noise signals running 20 times. The significance level acquired by this method has been compared with a trial-shifted surrogates method. The results from these two methods are nearly identical (Lachaux et al., 2002).

4.2.2 Simulation

4.2.2.1 Simulation Datasets

The wavelet coherence between two simulated signals was tested on two sets of simulation data. The first simulated data set was to test if the wavelet coherence could track the dynamic coherence changes within single trial. One signal (Fig. 4.2a) was the 25Hz sine from 1.67s to 3.3s buried in Gaussian distributed random signals (mean=0, σ =1). The other signal set (Fig.4.2b) contained the 25Hz sine from 1s to 3s buried in Gaussian distributed random signals (mean=0, σ =1). Both signals had a signal-to-noise ratio of 1. The time varying wavelet coherence was calculated with N_{co}= 6 and N_{cy}= 8. Then the local non-stationary components (amplitude modulation) was added to the first signal (Fig.4.2e). The time varying wavelet coherence was calculated again between this amplitude modulated signal and the second sine signal (Fig.4.2f).

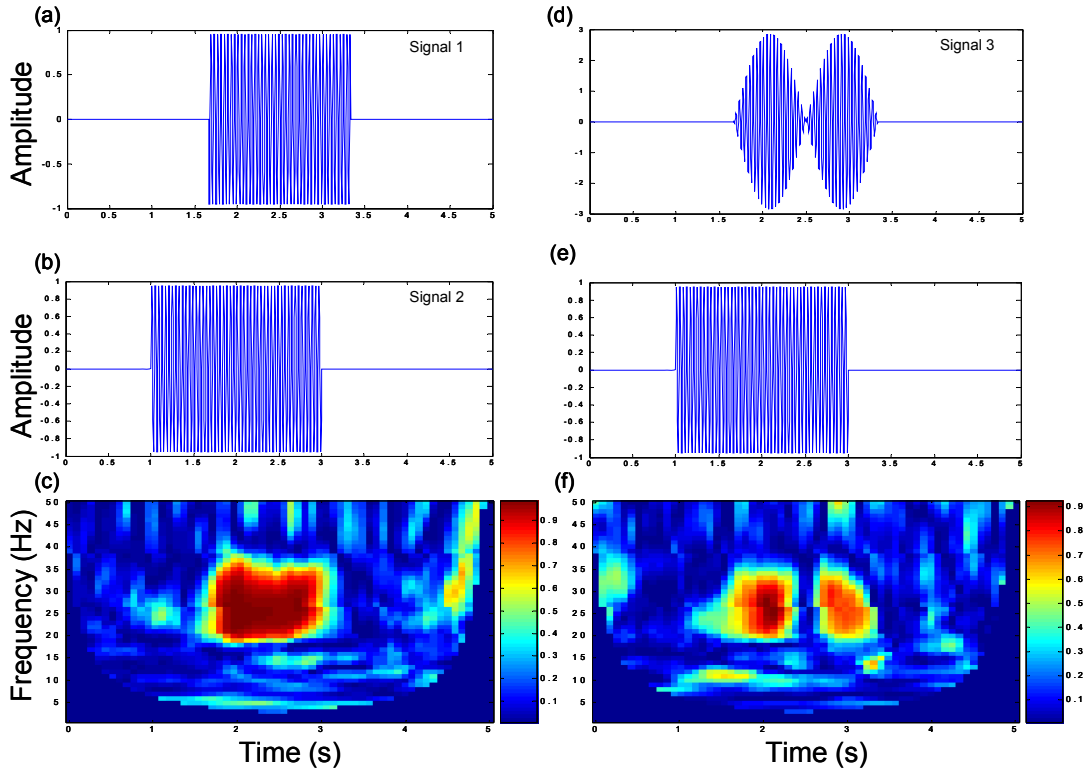

Fig. 4.2. Simulation results of time-frequency wavelet coherence for dataset 1. (a) 25Hz sine wave from 1.67s to 3.33s that was included in the simulation signal 1 (SNR=1); (b) 25 Hz sine signal from 1s to 3s that was included in the simulation signal 2 (SNR=1); (c) The time-frequency distribution of the wavelet coherence of signal 1 and signal 2; (d) 25Hz sine signal from 1.67s to 3.33s with amplitude modulation that was included in the simulation signal 3 (SNR=1); (e) 25 Hz sine signal from 1s to 3s that was included in the simulation signal 2 (SNR=1); (f) The time-frequency distribution of the wavelet coherence of signal 3 and signal 2.

Further simulation was tested on two 150-trial (2s/trial), signals (Fig.4.3 simulation dataset 2) to verify its ability to track dynamic coherence changes within a single trial and across a small number of trials. Each trial of signal B was a 25Hz sine from 0.28s to 1.71s buried in Gaussian distributed random signals (mean=0, σ =1). Signal A in each trial also included the 25Hz sine started from 0.28s buried in random signals (mean=0, σ =1). The duration of 25Hz sine signal was linearly increased from 0.01s to 1.43s from trial 1 to trial 75 and decreased from 1.43s to 0.01s from trial 76 to trial 150. The signal-to-noise-ratio of signals A and B in each trial was 1. Both single trial wavelet-based

coherence and FFT-based coherence for two blocks (block1: trial 1-trial 75; block2: trial 76-trial 150) were calculated and compared.

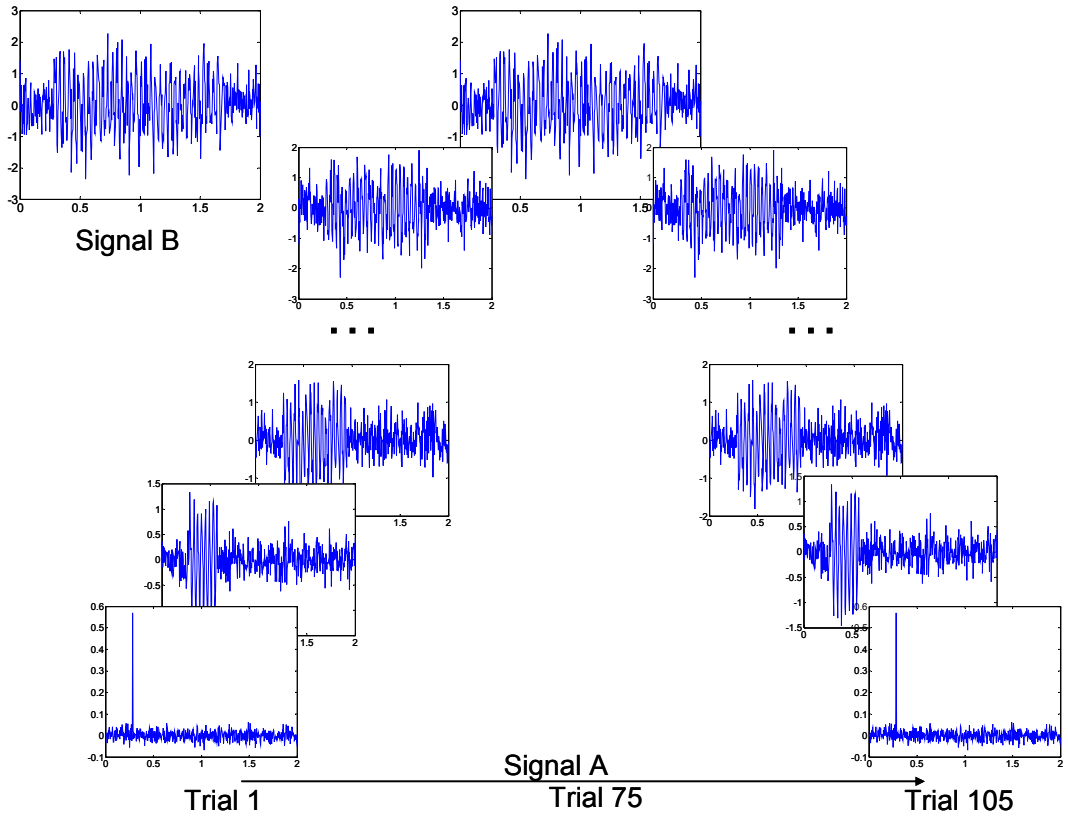

Fig. 4.3. Simulation dataset 2: signal B, 25Hz sine from 0.28s to 1.71s buried in Gaussian distributed random signals (mean=0, σ=1) with SNR=1 for each trial; signal A, each trial also included 25Hz sine started from 0.28s and random signal (mean=0, σ=1) with SNR=1 for each trial, but the duration of 25Hz sine signal was evenly increased from 0.01s to 1.43s from trial 1 to trial 75 and decreased from 1.43s to 0.01s from trial 76 to trial 150.

4.2.2.2 Simulation Results

The third row of Fig. 4.2 shows the results of the time-frequency distribution of the wavelet coherence for simulation Dataset 1. The wavelet coherence correctly tracked the coherence changes with time, especially when one of the signals was added with non-stationary component (Fig. 4.2f).

The simulation results of dataset 2 are shown in Fig. 4.4. Fig. 4.4a was the FFT-based coherence spectra of two blocks (block 1: trials 1-75; block 2: trials 76-150). There

was no difference in the coherence for the two blocks. Fig. 4.4b shows results of single trial wavelet coherence values at 25 Hz plotted as a function of trial. The single trial wavelet coherence value at 25 Hz was determined by averaging coherence values over time points throughout the trial. The single trial wavelet analysis correctly detected the coherence of the individual trials which could not easily be seen by using traditional FFT-based methods.

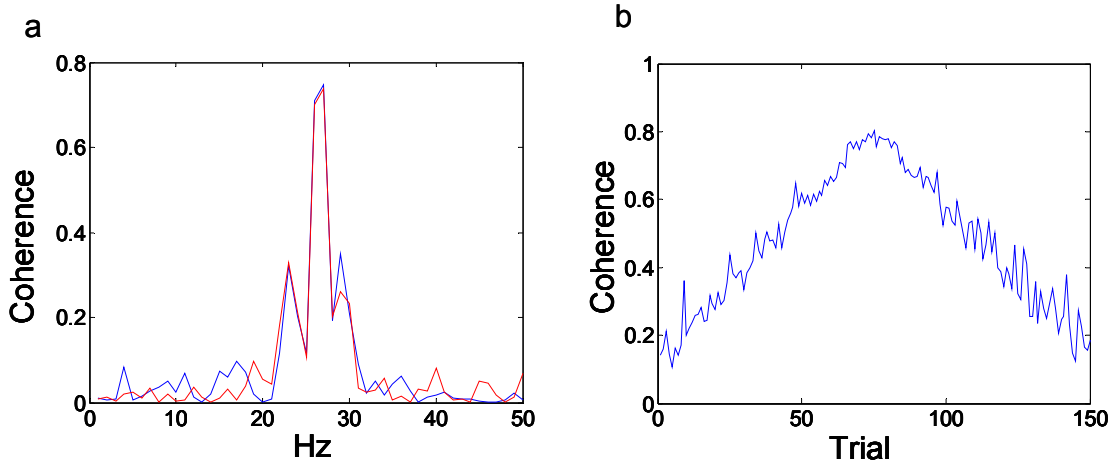

Fig. 4.4. Simulation results of simulation dataset 2. (a) FFT-based coherence spectra for two blocks (block 1: blue, block 2: red); (b) results of single trial wavelet coherence values at 25Hz plotted against trial.

4.2.3 Experiment

Eight healthy subjects participated in the study (7 men and 1 woman, age = 32.7 ± 7.7 years, all right-handed). The experimental procedures were approved by the Institutional Review Board at the Cleveland Clinic. All subjects gave informed consent prior to their participation. Each subject performed 200 intermittent maximal handgrip contractions of the right arm in a single session (Fig. 4.5). Each contraction lasted 2s followed by a 5s rest period. To maintain the correct timing of a contraction, subjects followed visual cues that were displayed on an oscilloscope screen. The visual cues were

a series of traveling rectangular pulses (Fig. 4.5a), each of which was 2 s with a 5-s interval between pulses. The height of the pulses represented the amplitude of the maximal handgrip force of the subject, which was measured at the beginning of the experiment. Subjects performed each trial by following the shape of the rectangular pulse. They were asked to exert the maximal force while avoiding unnecessary body movements. The force, EMG, and EEG data (Figs. 4.5b, c, and d, respectively) were recorded simultaneously.

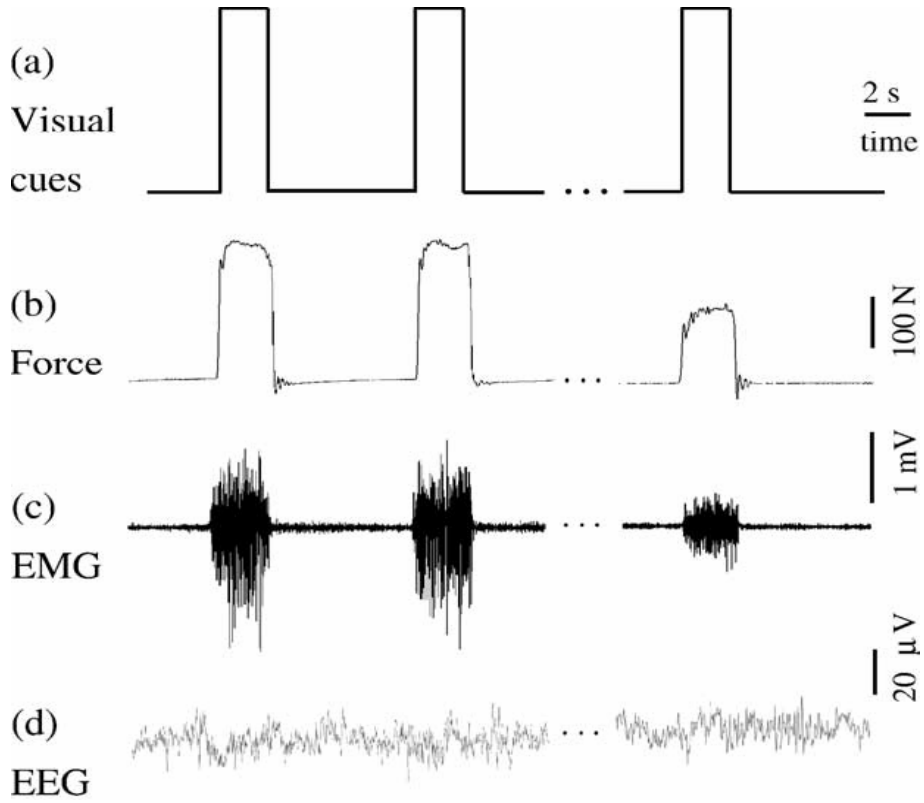

Fig. 4.5. Illustration of the experimental protocols. (a) The visual cues that were displayed on an oscilloscope screen to guide the handgrip contractions. Each contraction lasted 2 s, and the rest period between two contractions was 5 s. (b) A sample period of force time course, which showed a close match between the visual cues and the actual performance by the subject. (c) The corresponding raw EMG data in one channel. (d) The corresponding raw EEG data in one channel. J.Z. Liu et al. / Brain Research 1057 (2005) 113– 114 126

Subjects gripped a bottle-like soft plastic device that was connected to a pressure transducer (EPX-N1 250 PSI, Entran Devices, Inc., Fairfield, NJ) by a nylon tube filled

with distilled water (Liu et al., 2000, Liu et al., 2002). The force applied by the hand was sensed and converted to a voltage signal by the pressure transducer located in a sealed hydraulic environment. The output of the transducer was directed to a custom-built amplifier and then to an input channel of the Spike 2 data acquisition board (version 3.05, Cambridge Electronic Design, Ltd., Cambridge, UK), which transferred the voltage data to a computer. The sampling rate for the force data was 100 Hz. A sampled time course of the force is displayed in Fig. 4.5b.

Surface EMG signals were recorded using the Neurodata Amplifier System (Model 15A, Grass-Telefactor, West Warwick, RI) from the following 10 muscles, including both the prime and non-prime movers and their antagonists: flexor digitorum superficialis (FDS), flexor digitorum profundus (FDP), extensor digitorum (ED) of the right arm, and FDS, ED, and BB of the non-performing left arm. The reason for recording the EMG from the non-prime movers in the right arm (BB, DT, and TB) and muscles of the left arm (FDS, ED, and BB) was to monitor possible fatigue-induced activities in these muscles. The muscles were identified by palpating the muscles, while subjects moved the appropriate joints. Bipolar electrodes (Ag–AgCl, 8-mm recording diameter, In Vivo Metric, Healdsburg, CA) were attached on skin overlaying each muscle. A reference electrode was placed on the skin overlying the lateral epicondyle near the elbow joint of the right arm. The EMG data were amplified (x1000), band-pass filtered (1–1000 Hz bandwidth), and recorded at a sampling rate of 2000 Hz to the computer by the Spike 2 data acquisition system.

EEG signals were recorded from the scalp using a 64-channel NeuroSoft SYNAMPS system (version 4.2, Neuro-Scan, El Paso, Texas, USA). The subjects were

seated in a position that allowed them to perform the handgrip task comfortably. The electrode cap that holds the 64 Ag–AgCl electrodes was placed onto each subject's head, based on the International 10–20 positioning method. Conducting gel (Electro-gelTM, Electro-Cap International, Inc., Eaton, OH, USA) was injected into the electrodes to connect the recording surface of each electrode with the scalp. The impedance of the EEG channels was maintained below 10 KV. One of the 64 electrodes (O2) was used to record the handgrip force. All the remaining 63 electrodes were referenced to the linked mastoids (M1 and M2). The EEG signals were band-pass filtered (0.05–50 Hz), amplified (x75,000), and recorded on the hard disk of the computer at a sampling rate of 250Hz. The subjects were required to concentrate on the task performance and minimize distractions as much as possible. They were asked to maintain a stable body position and avoid eye blinks, teeth biting and head movements during the handgrip contractions, whereas minimal eye blinks and body adjustment were allowed during the relaxation periods. Possible sources of distraction or noise, such as sound or light, were minimized. In Fig. 4.5d, sample EEG data in one channel corresponding to the force/EMG data in Figs. 4.5b–c are displayed.

4.2.4 Data Analysis

Although subjects were advised not to blink eyes, clench teeth, move head, or tense muscles other than those involved in the handgrip contractions, these activities occasionally occurred, and the trials associated with these activities were excluded from further analysis. These trials were identified by visually inspecting all raw EEG data. On average, each subject has 174±7 trials EEG data (ranged from 152 to 197 trials) that were artifact-free. To facilitate the further data analysis, only first 150 artifact-free trials of

each subject were subjected to subsequent analysis.

Two measurements were made for each trial of the EEG and EMG data: the EEG-EMG wavelet coherence and wavelet energy spectra of the EEG and EMG signals during the 2s sustained phase of the muscle contraction. For each trial, the time varying wavelet coherence was acquired and the number of frequency bins that had significant EEG-EMG coherence was summed up as a function of time (1Hz per bin), which means that the time effect within the 2s trial was ignored because the study was more interested in comparing coherence of a later trial with that of an earlier one rather than doing that within the trial. Two parameters are needed to be determined in calculating wavelet coherence. Nco, the number of cycles of Morlet wavelets, was selected as 6 and Ncy, the smooth cycles in the integration window was 8, which defined the time resolution of the wavelet coherence as Ncy / f. (For example, when f = 15, time resolution was 0.53 s; when f = 30, time resolution was 0.27 s.) The number of bins with coherence above significance level was then summed in each frequency band (alpha (8-14Hz), beta (15-35Hz) and gamma (36-50Hz). Since the coherence at beta (15-35Hz) frequency band was more prominent, only coherence and wavelet energy spectrum at this frequency band were further analyzed. The wavelet energy spectrum in each trial was calculated at each time point and averaged across time at each frequency within the trial. The summed wavelet energy at beta band was subsequently normalized by the total energy summed from 1-50Hz and averaged across trials in each subject. The wavelet energy spectrum was calculated for each of the five motor related EEG channels located at five distinct motor function-related cortical areas (C3, C4, Cz, Fz and Pz) and two major finger flexor muscle EMG channels (FDS, FDP). The wavelet coherence was determined for each pair of EEG and EMG channels

among the five EEG and two EMG electrodes.

Following determination of the EEG-EMG coherence in each trial, a mean significant coherence bin number for each of the two blocks (75 trials in each block), five blocks (30 trials in each block) and ten blocks (15 trials in each block) was calculated, which allowed to detect fatigue effect on the coherence at different time scales. At each scale, a general linear model of repeated measures was fitted to determine how muscle fatigue affected EEG-EMG coherence.

4.3 Results

4.3.1 Muscle Fatigue indicated by Force and EMG Reductions

The subjects performed 200 trials of maximal voluntary handgrip contractions while the handgrip force and EMG of the finger flexor and extensor muscles were recorded. The amplitude of the force and EMG of each muscle was quantified across each block of 20 trials to yield 10 data points (Fig 4.6). Both the force and EMG declined significantly as more trials were performed, indicating significant muscle fatigue (Fig. 4.6).

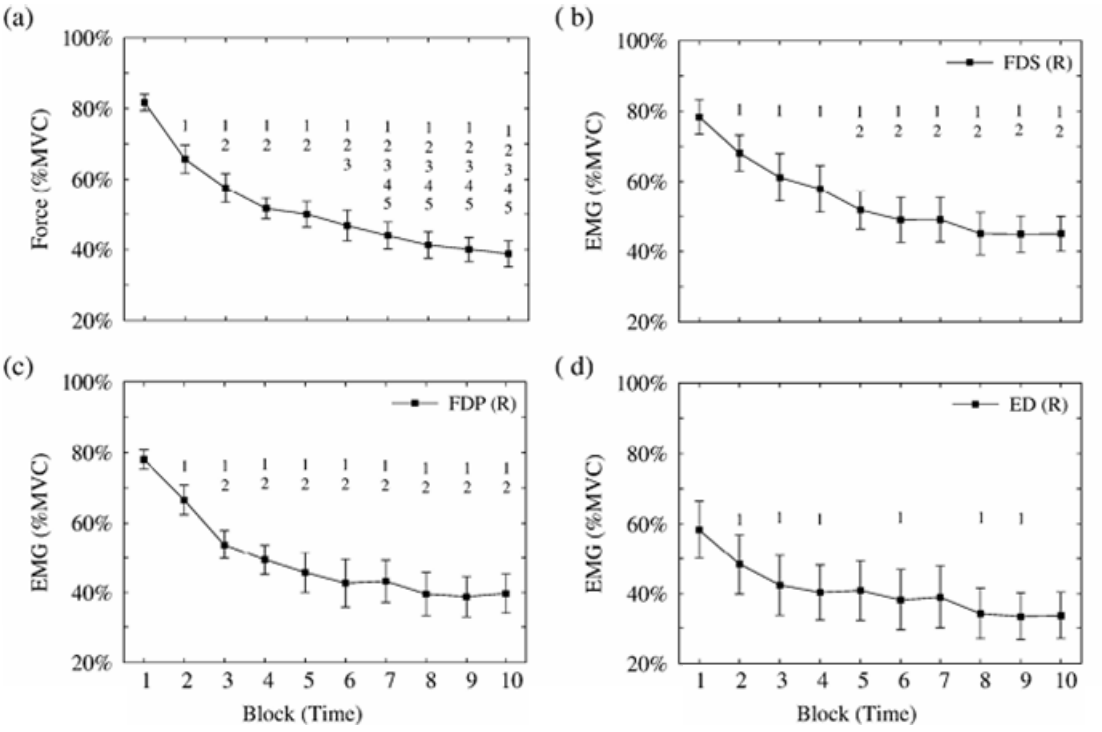

Fig. 4.6. Normalized force and EMG signals averaged over the eight subjects. (a) Handgrip force; (b–d) EMG signals from the prime movers (i.e., FDS, FDP) and the antagonist (ED) of the right (performing) arm; Each data point represents the averaged results over 20 consecutive handgrip contractions. Each numeral number within plot a, b, c, or d above a given data point indicates a significant difference ($P<0.05$) between this data point and the one corresponding to the numeral number. For example, the numeral ‘‘1’’ above block 2 in Fig. 4a indicates a significant decrease in the force of block 2 from the value of block 1. Similarly, the numeral ‘‘4’’ above block 7 suggests a significant force decrease in block 7 from that in block 4, and so on. J.Z. Liu et al. / Brain Research 1057 (2005) 113– 114 126

4.3.2 EEG-EMG Coherence and Energy Spectra

Fig. 4.7 shows trial-frequency distribution of the EEG (C4) and EMG (FDP) wavelet energy spectrum, and the EEG-EMG (C4-FDP) coherence spectrum in a typical subject. The highest EEG-EMG coherence (Fig. 4.7a) was found mainly at the beta band (15Hz-35Hz). The EEG-EMG coherence at the beta band decreased during the later trials (trials 90-150). The EEG wavelet energy declined gradually throughout the 150-trial data set with the highest value occurred around the 30^{th} trial (Fig. 4.7b). The EMG wavelet energy increased a little at the very beginning, maintained the highest level of energy

from the 25th to 60th trials and decreased sharply thereafter (Fig. 4.7c). The EEG and EMG wavelet energy change as a result of muscle fatigue were consistent with previous reports of the effect of muscle fatigue on EEG and EMG FFT power spectra adaptations (Liu et al., 2005).

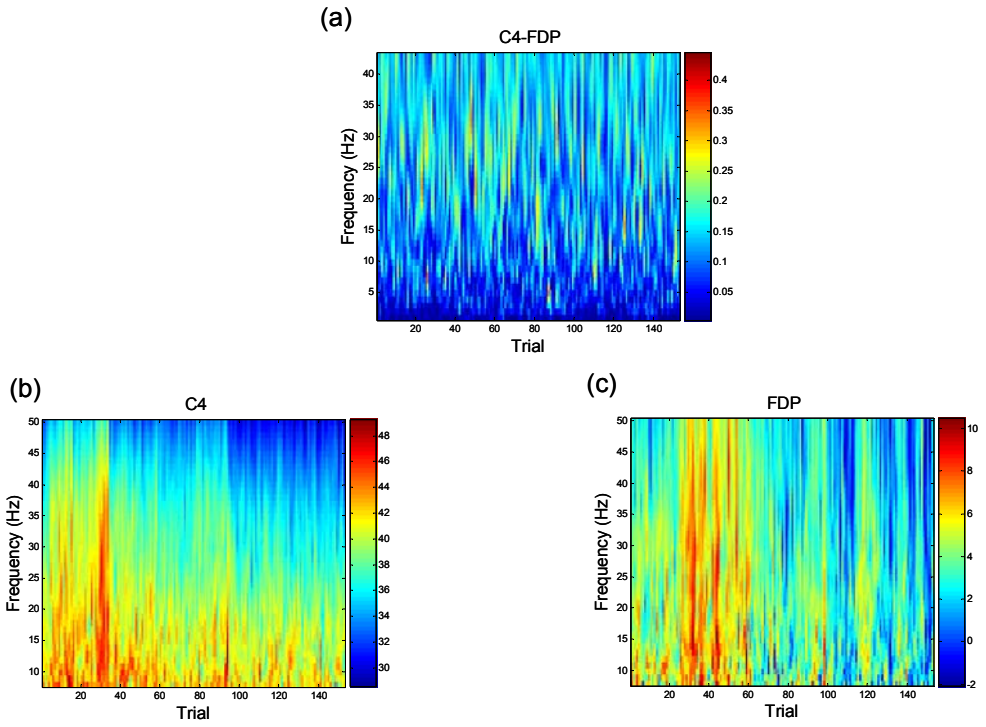

Fig. 4.7. The trial-frequency distribution of the EEG (C4) (b) and EMG (FDP) (c) wavelet energy spectra with color bars indicating the normalized wavelet energy value; the EEG-EMG (C4-FDP) (a) coherence spectrum in one of the typical subjects with color bars indicating the coherence value.

Figure 4.8 shows normalized wavelet energy spectra of the EEG (upper row) and EMG (lower row) signals based on group results. All the EEG channels had a similar trend of energy reduction across the trials. EMG energy in the FDS and FDP, the primary finger flexion muscles also had sharp reduction after about 30 (FDS) or 60 (FDP) trials of the contractions. Fig. 4.9 shows group results of the EEG (left column) and EMG (right column) energy spectra at beta band quantified and averaged across trials in 2 blocks (top row), 5 blocks (mid row) and 10 blocks (bottom row). For n blocks, the result of each

block was based on the average results of the 1/n total 150 trials (for example, 75 trials in each block for 2 block setting). Both the EEG and EMG energy decreased significantly in the 2 block setting and decreased gradually in the 5 and 10 block settings. Apparently, the 5- and 10-block results provided more information regarding the EEG and EMG signal responses to muscle fatigue.

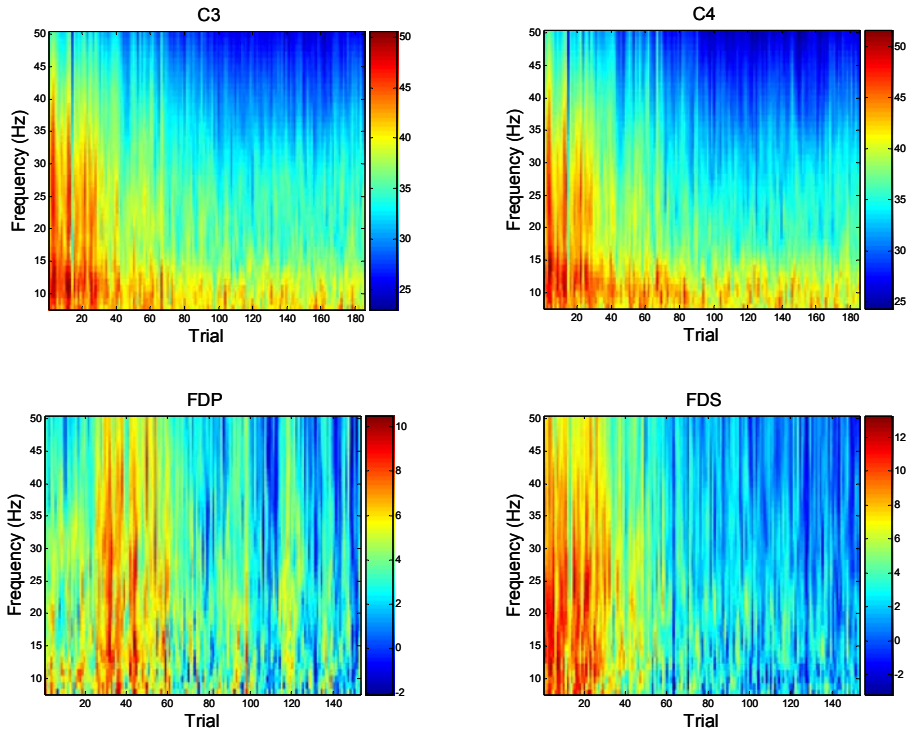

Fig. 4.8. Trial-frequency distribution of the EEG (C3 and C4), EMG (FDS, FDP and ED) normalized wavelet energy spectra averaged across the eight subjects. The wavelet energy was normalized by the corresponding total energy summed from 1-50Hz and averaged across trials in each subject.

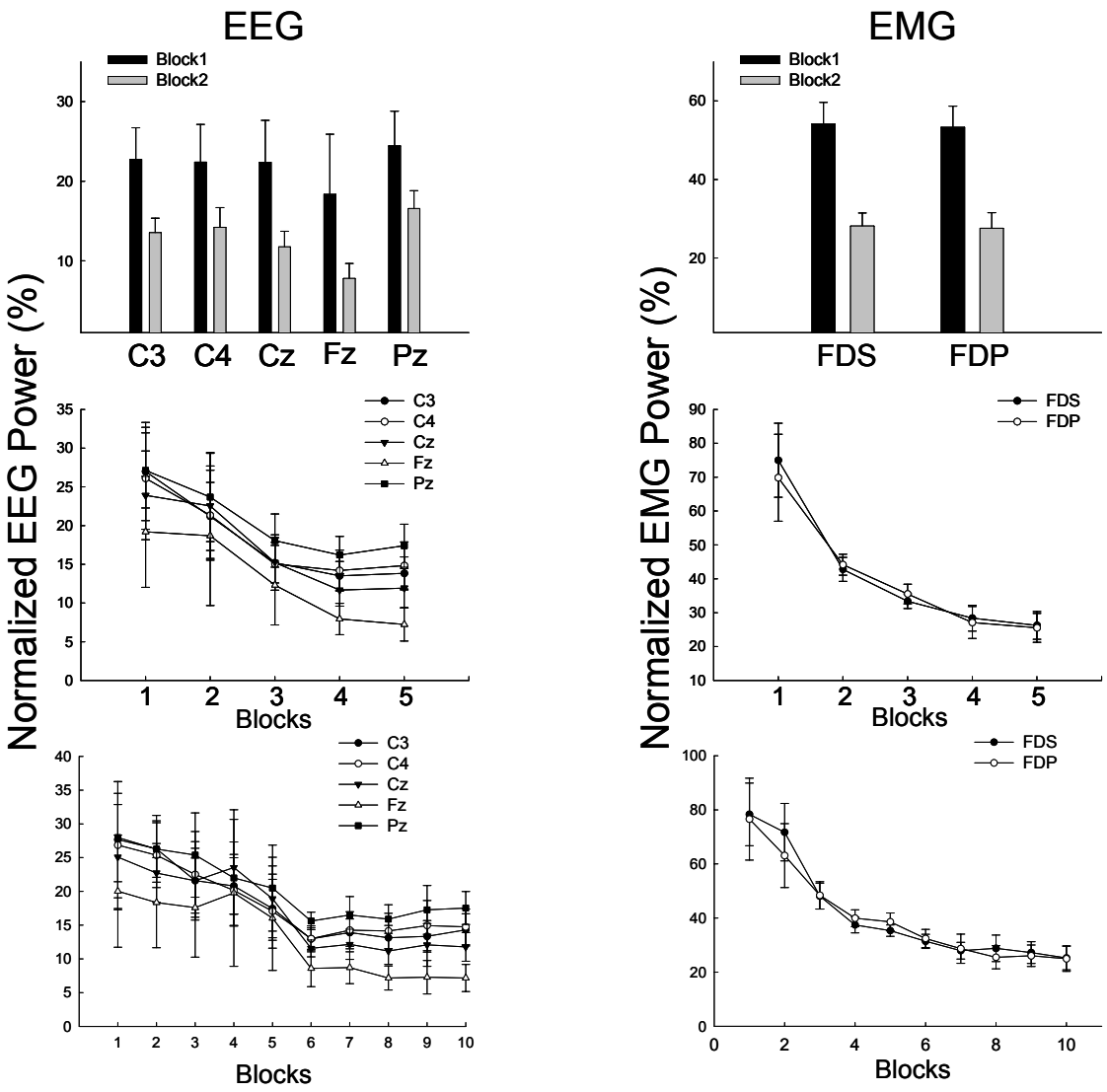

Fig. 4.9. The average results of the beta band (15-35Hz) EEG (left row) and EMG (right row) energy spectra quantified in 2 blocks (first row), 5 blocks (second row) and 10 blocks (third row). The results were the summed normalized energy in beta band and averaged across trials and subjects within each block.

Fig. 4.10 shows group results of the beta band (15-35Hz) single trial EEG-EMG coherence averaged across trials in 2 blocks (first row), 5 blocks (second row) and 10 blocks (third row). Comparing results between the two blocks, the coherence (number of frequency bins having significant EEG-EMG coherence between the specified EEG electrodes and EMG of the FDP muscle) decreased significantly ($P<0.01$). In the five-block setting, the coherence hit the lowest in block 4 for both the muscles but the trend of

decrease was clearer for the coherence of FDS EMG with the selected EEG channels. In the ten-block setting, the change pattern of EEG-EMG coherence was similar to that in the 5-block setting for both the muscle except that more detailed information was revealed in the 10-block data. Two trial-frequency distribution maps of EEG-EMG coherence in two subjects are shown in Fig. 4.11. Each map showed a decreasing trend of in the coherence, but the pattern of change was different from one subject to the other.

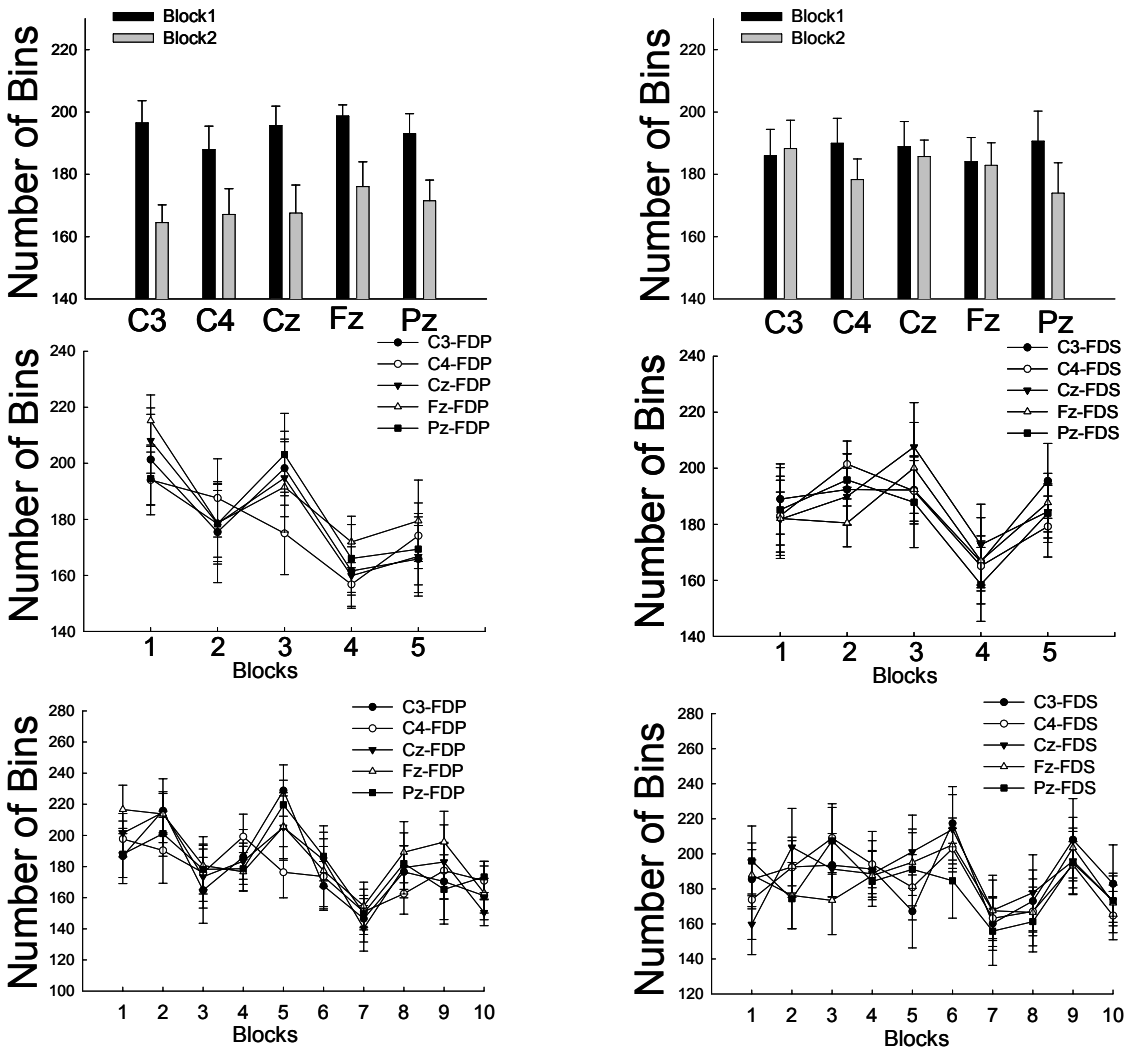

Fig. 4.10. The average results of the beta band (15-35Hz) EEG (C3, C4, Cz, Fz, Pz)-EMG (FDP (left column), FDS) wavelet coherence quantified in 2 blocks (first row), 5 blocks (second row) and 10 blocks (third row). The results were the summed normalized energy in beta band and averaged across trials and subjects within each block.

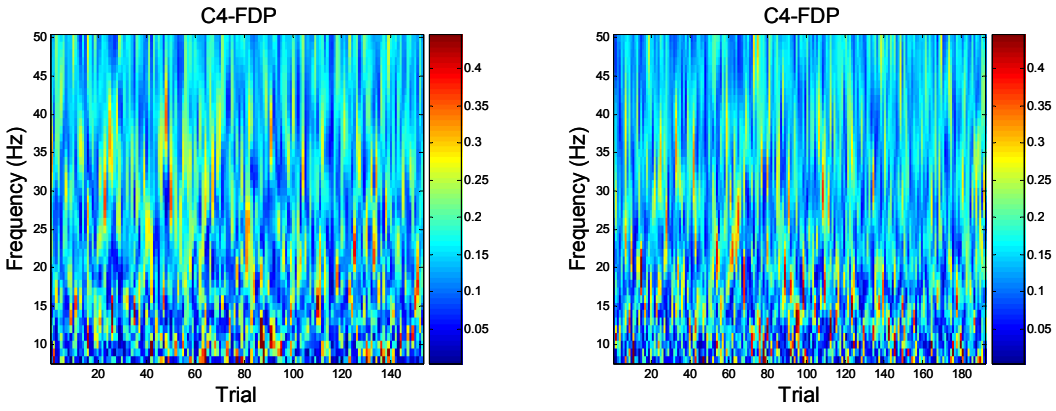

Fig. 4.11. The trial-frequency distribution of the C4 EEG-FDP EMG wavelet coherence spectra of two subjects.

4.4 Discussion

This study demonstrated feasibility of quantifying single-trial EEG-EMG coherence to detect muscle fatigue effect on functional corticomuscular coupling. Although the gross (2 block) analysis showed that the coherence decreased significantly from the first trial-block to the second trial-bock. The single trial coherence analysis revealed substantially more information regarding the timing of the coherence change with muscle fatigue and variation of the measurement among the subjects.

Functional corticomuscular coupling in beta band that measures binding strength between the brain and muscle, has been suggested to be directly related to the motor parameters of the performed tasks (Kilner et al., 2000). Functional corticomuscular coupling is frequently quantified by brain and muscle signal coherence. It has been found that the EEG-EMG coherence decreased significantly from less-fatigue stage to severe-fatigue stage in a submaximal sustained muscle contraction (see chapter 2). However, only one FFT-based coherence spectrum was calculated for the data in each stage of a relatively long time span, which made it impossible to learn the time course of the

coherence change on a much finer scale. In this study, the multiple trials (150) of maximal handgrip contractions were performed by human subjects and single trial coherence between the EEG collected from motor and sensory cortical regions and EMG of the finger flexor muscles was calculated. The single-trial results confirmed the previous findings: the EEG-EMG coherence declines significantly with fatigue (from less-fatigue stage to severe-fatigue stage) (Fig.4.10 top row). The EEG and EMG wavelet energy decreases with fatigue as well (Fig.4.9 top row). Weakening of functional corticomuscular coupling could be due to fatigue-related increases in inhibitory drive to the descending motor passway, a decrease in neuromuscular junction transmission function, and shifting of primary output centers in the brain, which has been explained in the previous chapter.

In addition to the above findings, more information was revealed from single-trial coherence analysis. The change pattern of the coherence quantified within five blocks (Fig.4.10 mid row) or ten blocks (Fig.4.10 bottom row) showed that the lowest coherence did not occur at the last block but at an earlier time. Also the decreasing EEG and EMG wavelet energy plateaued at the last two or three blocks. It has been reported that during a sustained isometric maximal contraction, motor evoked potential elicited by transcranial magnetic stimulation increased at the first 10-15s of the contraction and leveled off later (Taylor and Gandevia, 2001). The flattening of the EEG wavelet energy reduction may be explained by plateau of motor unit firing rate or recruitment after the initial rapid decline (Gandevia, 2001). However, whether the plateau of EEG-EMG coherence was related to the EEG energy plateau is unclear. It was noticeable that the EEG-EMG coherence increased to the highest level at the middle block of the muscle contractions,

which was not seen in the EEG or EMG wavelet energy time course. The other additional information that can be obtained from the single trial coherence analysis is that each subject showed a unique pattern of dynamic coherence adaptation as a function of fatigue although the overall change trend was the same. The coherence variation among subjects was relative big across the trials within each block; for this reason the difference in the coherence in the 5-block or 10-block conditions was not significantly different among the blocks.

Wavelet analysis, the alternative of the Short-Time Fourier Transform (STFT), has been known to provide a better compromise between time and frequency resolution (Tallon-Baudry et al., 1997) and may be a useful approach in investigating non-stationary signals, such as EEG (Senhadji et al., 1995, Samar, 1999, Goelz et al., 2000, Merzagora et al., 2006, Chen et al., 2007) and EMG (Xiao and Leung, 1997, Flanders, 2002, Leao and Burne, 2004). It is particularly useful for short-duration signals commonly seen in neuroscience research. In this case, STFT method is with limitation of losing accuracy in the frequency component. In the recent years, a number of studies have applied the wavelet-based coherence analysis to address neurophysiological issues (Lee, 2002, Ayoubian Markazi et al., 2005, Li et al., 2005, Klein et al., 2006, Zhan et al., 2006). The wavelet coherence acquired by smoothing multiple trials (Zhan et al., 2006) has been tested as comparable to the STFT based coherence. However, single-trial wavelet coherence is considered more suitable for fatigue studies with intermittent trials of muscle activation. This is because the assumption of each repeated trial having the same physiological activity at the same latency apparently does not hold for progressive muscle fatigue. Physiological responses during fatigue change substantially even in a short time.

Smoothing within a trial allows wavelet coherence to be estimated for the given trial (Torrence, 1999, Lachaux et al., 2002, Brittain et al., 2007). Three methods, smoothing by time (Lachaux et al., 2002), scale-dependent 2-D smooth operator (Torrence, 1999) and multiwavelet (Brittain et al., 2007) have been proposed to estimate the time-frequency wavelet coherence in single trial. It is unclear in what direction the smoothing should be done (Torrence and Compo, 1998). We chose the method of smoothing in time within each trial: the 2 second holding period of the muscle contraction. This method was first tested using simulated data, and found that the method could correctly track the dynamical coherence changes within the trial and across the trials. Since this method requires the data to be smoothed within time, it needs a minimal duration of time in each trial. A two-second duration is adequate for 8 Hz and higher frequency wavelet coherence estimation under the current parameter setup. If lower frequency wavelet coherence is of interest, longer duration trials are needed. Adjusting the current parameters (integration window number and number of cycles of Morlet wavelets) would not help because the integration window number parameter is unlikely to decrease. Alternatively, the multiwavelet smoothing method can be considered. The single trial coherence estimation can be further implemented in real time application for detecting the coherence and power spectra.

In conclusion, single trial wavelet coherence and wavelet power spectrum were useful to analyze muscle fatigue effect on functional corticomuscular coupling (EEG-EMG coherence): both wavelet coherence and power spectrum decreased with fatigue. However, different subjects and muscles exhibited different reduction patterns. The

single-trial analysis also provided more information regarding dynamic adaptation of the brain signal and functional corticomuscular coupling during muscle fatigue.

CHAPTER V

TIME-FREQUENCY TEMPLATE MATCHING METHOD FOR CLASSIFYING MOTOR IMAGERY IN BRAIN COMPUTER INTERFACE

5.1 Introduction

The brain-computer interface (BCI) is ‘a real-time communication system that does not depend on normal output pathways from the brain to muscle through corticospinal and peripheral nerve connections’(Wolpaw et al., 2002). It provides ‘locked-in’ patients a new channel of communication (Fig 5.1). Various invasive and non-invasive BCI approaches have been developed. However, noninvasive BCI is preferable among the users, considering many practical application reasons. Among various non-invasive BCI systems, one category of BCI is based on surface EEG pattern recognition of different cognitive tasks. It assumes that differentiated cognitive tasks, especially motor imagery

tasks, would lead to distinct and detectable distribution of EEG spatial and spectral patterns over the scalp. Motor imagery tasks usually lead to a frequency power decrease in mu (8-14Hz) and beta (15 -35Hz) rhythms (event-related de-synchronization: ERD) in brain hemisphere contralateral to the movement (Fig 5.2). Event-related synchronization (ERS) occurs after movement when muscles are relaxing, which is prominent in the contralateral motor cortex (Pfurtscheller et al., 1996). A series of studies by Pfurtscheller's group have shown that mental imagery of specific movements of arms, fingers or legs led to different EEG frequency patterns, which could be used to control a BCI system (Kalcher et al., 1996).

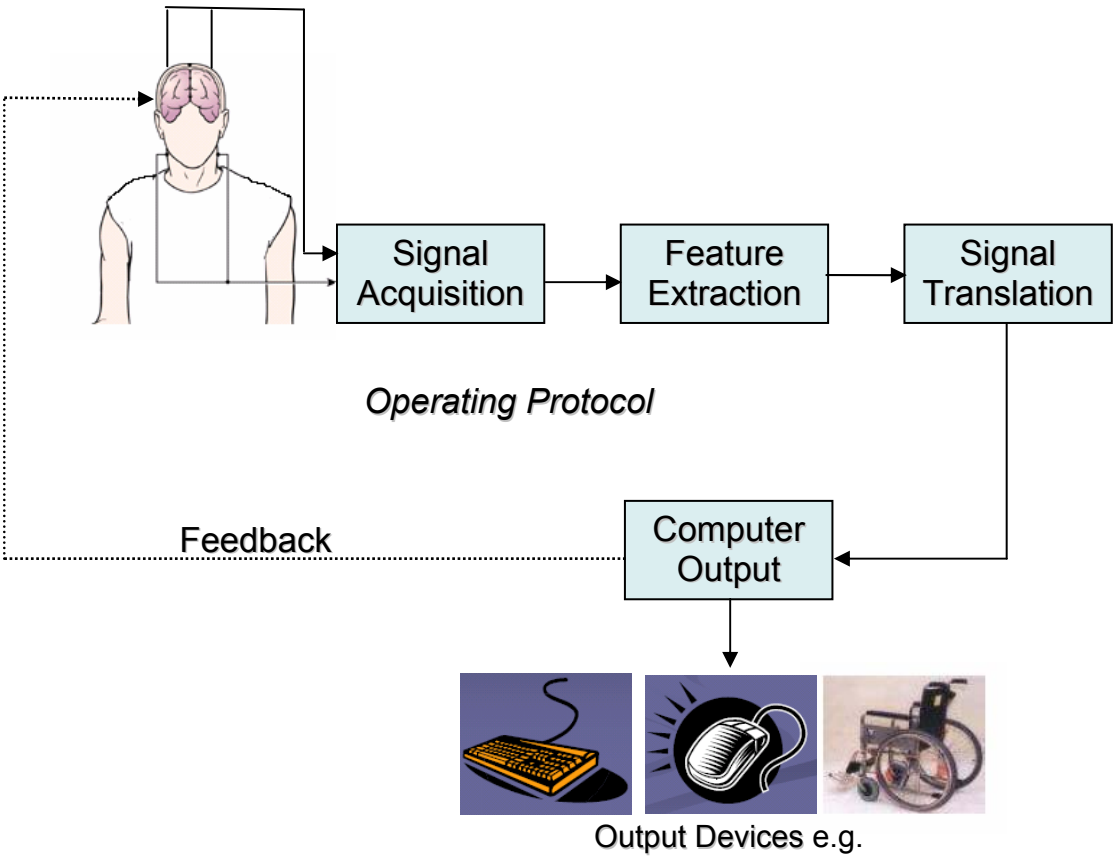

Fig.5.1. BCI system basic components

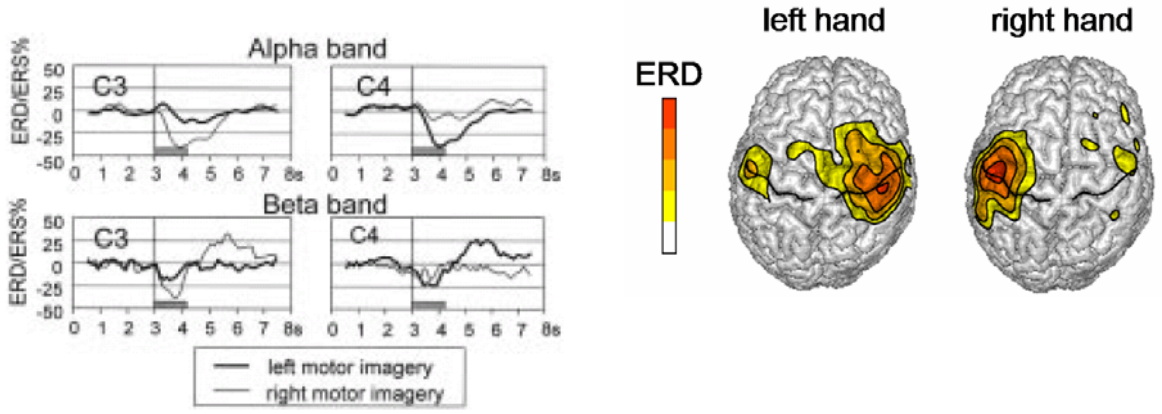

Fig.5.2. Event-related de-synchronization (ERD) difference between left and right hand movement imagination. Left part line figures: Grand average ERD/ERS curves recorded over left and right sensorimotor cortices during motor imagery. The ERD/ERS time courses were calculated for the selected bands in the alpha and beta range. Positive and negative deflections, with respect to the baseline, represent a band power increase (ERS) and decrease (ERD), respectively. The gray bar in each plot indicates the time period of cue presentation. Right part brain images: illustration of localization of upper-alpha band ERD of the left and right hands (Neuper et al., 1999).

Various methods have been developed to extract and classify the ERD and ERS patterns. Autoregressive (AR) model based spectrum (Pfurtscheller et al., 1998), band powers combined with distinction sensitive learning vector quantization (DSLVQ) (Scherer et al., 2003), common spatial patterns (CSP) (Lemm et al., 2005) and phase synchronization (PS) (Brunner et al., 2006), source location (SL) (Qin et al., 2004, Kamousi et al., 2005), time-frequency (TF) analysis (Qin and He, 2005, Ince et al., 2006), or feature combination are the feature extraction methods that have been investigated. These feature extraction methods have been combined with different types of classifiers, including linear discriminant analysis (LDA), k-nearest-neighbor (kNN), support vector machine (SVM) and various neural networks to achieve good classification results. Many studies have shown that sophisticated signal processing algorithms are superior to simpler

techniques in offline analyses for potential BCI applications. However, the more complex the analysis is, the less amenable it might be for online BCI control involving real-time, continuous feedback and adaptation. Until now only four feature extraction methods (AR, DSLVQ, CSP, and PS) and LDA classifier have been implemented online. The AR method used a two-dimension-feature vector that formed by the AR coefficients of EEG data segment along the time to distinguish the different EEG pattern. The DSLVQ is a feature selection algorithm to identify the optimal band of frequencies that bear the largest difference between imageries of left and right hand movements. The CSP can be used for identifying the electrodes that provide better discriminatory information. The degree of phase synchronization between two EEG signals by calculating phase locking value was extracted in PS method. However, none of these online methods used time and frequency features simultaneously for the classification. However, the features of the ERD and ERS are apparently time, frequency and space related. This makes time frequency analysis based on wavelet transform a potentially useful approach to extract features of the ERD and ERS. Several TF methods have been developed and their applications on offline BCI have been reported (Bostanov, 2004, Qin et al., 2004, Glassman, 2005, Ince et al., 2006).

Here a modified time frequency template matching strategy based on method of Qin and He (Qin and He, 2005) was described. Offline and pilot online experiment results were reported. It was hypothesized that wavelet based time frequency extraction method would lead to higher accuracy and less user-training time for offline and online distinguishing signal patterns of the left and right hand movement imageries.

5.2 Methods

5.2.1 Algorithm

Step 1: EEG data from two channels (C3 and C4) were used (electrodes C3 and C4 overlay the left and right side of primary motor cortex). These data were first preprocessed by the laplacian spatial filter to enhance local activity (Hjorth, 1975). Assuming that the distances from the four surrounding electrodes to the electrode of interest are approximately equal, the surface Laplacian can be calculated as following:

$$v_j^{Lap} = v_j - \frac{1}{4}\sum_{k \in S_j} v_k \tag{5.1}$$

where Vj was the potential of the jth electrode, and Sj was an index set of the four surrounding electrodes.

Step 2: For each task (left and right hand movement imagery) and each channel (C3 and C4), the time-frequency (TF) distribution map was acquired through Morlet wavelet transform from each trial of the laplacian spatial filtered training EEG data.

Complex Morlet's wavelets have a Gaussian shape both in the time domain (SD σ_f) and frequency domain (SD σ_t) around its central frequency f_0 (Tallon-Baudry et al., 1997):

$$w(t, f_0) = A\exp(-t^2/2\sigma_t^2)\exp(2i\pi f_0 t) \tag{5.2}$$
$$\sigma_f = 1/2\pi\sigma_t \qquad f_0/\sigma_f = 7 \qquad A = (\sigma_t\sqrt{\pi})^{-1/2}$$

The time-varying energy of the signal in a frequency band was the square norm of the result of the convolution of the complex wavelet with the signal.

The ERD and ERS patterns were detected by averaging training data across trials. The C4 averaging TF map was subtracted from C3 averaging TF map; the subtraction outcome was dramatically different between the left hand movement imagery and the right hand movement imagery task. This C3-C4 TF energy distribution map was served as a template for each task.

Step 3: Training template matching indices based on un-normalized correlation coefficient from training data was calculated.

$$\rho(x,y) = \frac{\sum_{i=1}^{n}\sum_{j=1}^{m}(x_{ij} - \bar{x})y_{ij}}{\sqrt{\sum_{i=1}^{n}\sum_{j=1}^{m}(x_{ij} - \bar{x})^2}\sqrt{\sum_{i=1}^{n}\sum_{j=1}^{m}y_{ij}^2}} \tag{5.3}$$

i: time index; j: frequency index; x represented the single trial data, and y was the averaging template data.

Step 4: Testing template matching indices from testing data were calculated in the same way.

Step 5: Linear discriminant analysis classifier (LDA), which transforms the data by maximizing the ratio of between-class variance to the within-class variance, was used to classify these features to see if the testing trial TF pattern was more closely matched to the left or right template based on the input of the training template matching indices.

$$D = w^T x + w_0 \tag{5.4}$$

D was the distance: the magnitude of the value indicates the confidence of the classification; the sign indicates the class; x was the classified data; w, and w_0 were transforming weights obtained from the training data.

The whole algorithm flow chart is shown in Fig. 5.3.

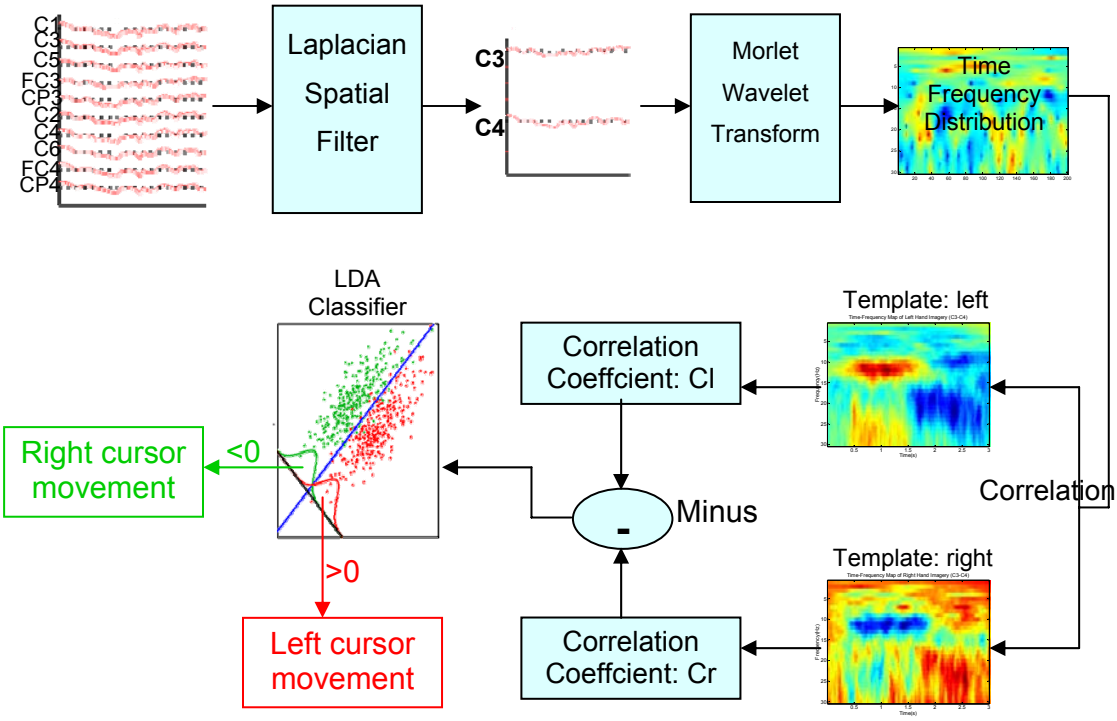

Fig. 5.3. Algorithm flow chart

5.2.2 Offline Experimental Protocol

So far no consensus exists on how to evaluate and compare the algorithms either online or offline. Several competitions have been organized so that algorithms from various groups could be applied to a given data set and evaluated by the same criteria (Sajda et al., 2003, Blankertz et al., 2004). Scalp EEG data of nine subjects from NIPS 2001 (conference of Neural Information Processing Systems competition) were provided by Dr. Allen Osman at the University of Pennsylvania (Parra et al., 2002) and were analyzed in this study. The signals were acquired using 59 electrodes positioned on the scalp according to the International 10/20 system with a sampling rate of 100 Hz. The data were recorded during performance of a total of 180 trials of an imagery hand

movement (imaging right/left hand movement without actual doing it), 90 trials for the left hand and 90 for the right hand. Each trial (6 s) began with a blank screen lasting for 2 s. After 1.75s preparation time, at t=0 s, a preparation cue of letter 'L' or 'R' (lasting 250 ms) appeared on the screen indicating which hand movement should be imagined; at t=1.25s an execution cue 'X' (lasting 50 ms) appeared, telling the subject to make the requested imagery for 1s. The experimental paradigm described above is shown in Fig. 5.4.

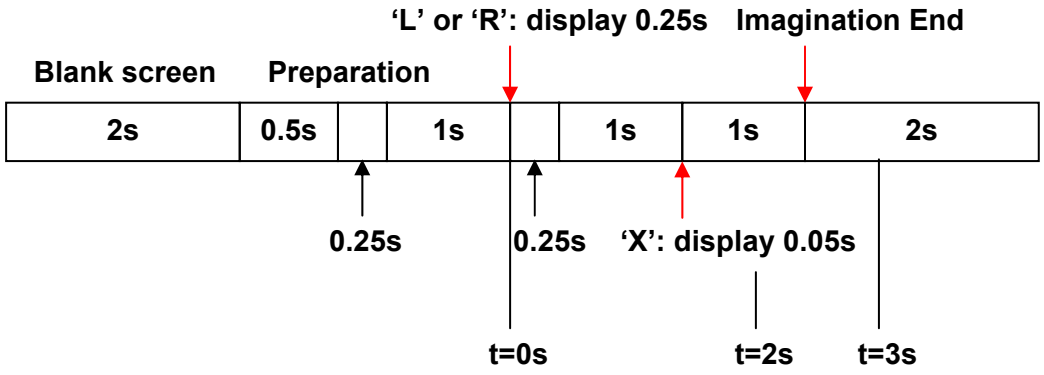

Fig. 5.4. Offline experiment paradigm

Time-frequency (TF) distribution map was acquired through Morlet wavelet transform for the interested time period (0-3s) and channels (C3 and C4) of the Laplacian spatial filtered training EEG data signal. Clear ERD and ERS patterns could be detected by averaging all left/right training data. This averaging TF energy distribution map was served as a left/right template. One typical subject's TF distribution map is shown in Fig. 5.5, which shows distinct ERD and ERS patterns for the imagery movements of the left and right hand. Template matching technique based on correlation coefficient was used to extract coefficient feature by comparing the testing trial with the average left and right template. LDA classifier was used to classify these features to see if the testing trial TF

pattern was more closely matched to the left or right template. This classifier result was compared to the original test data tag. If they matched, the classifier result was accurate.

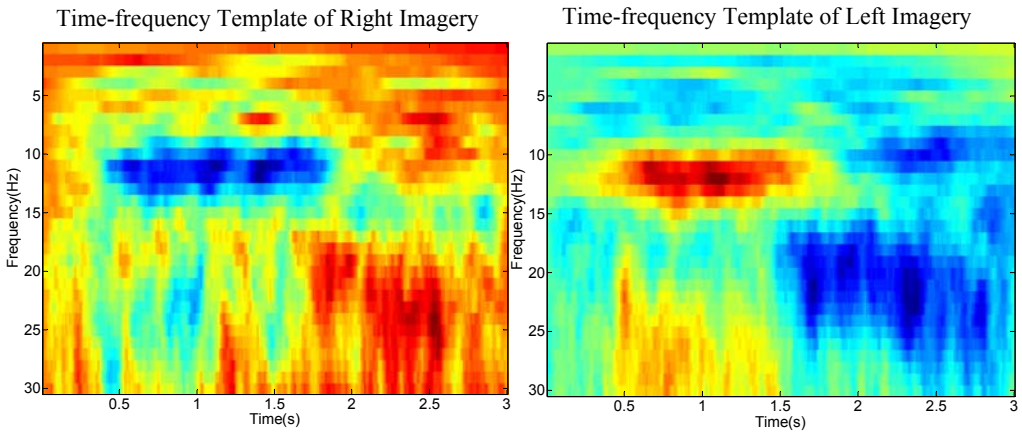

Fig. 5.5. TF energy distribution map of one typical subject, averaged across 90 imagery trials of the left hand and 90 imagery trials of the right hand movements. Red means higher amplitude and blue means lower amplitude of the signal wavelet energy.

5.2.3 Online Experimental Protocol

Four subjects (1 female and 3 male, average age: 32.3±3.2 years) took part in the online experiment. One subject had four sessions of a previous version BCI training experience. The other three subjects had no prior experience or knowledge of BCI experiment. One subject reported that he could not concentrate and perform the imagery well. For this reason, this subject's data were excluded from the analysis. The EEG signals were acquired by a 64-channel Neuroscan system (version 4.2, NeuroScan, El Paso, Texas, USA) and bandpass filtered at 0.05-50 Hz. The sampling rate was 200 Hz. Subjects sat in a comfortable chair with both arms placed on the table or armrests, facing the screen. The subjects were given verbal instructions for correct metal practice after having several trials of actual hand movement practice (Sidaway and Trzaska, 2005).

The whole task performed in the online experiment was a basket game. In each trial, the initial screen was blank. After 800 ms, one of two rectangle targets (left and right) appeared at the bottom left or right of the screen, which was the preparation cue lasting several seconds (preparation time) depending on the individual subject. The side of the target was randomly selected. The cursor then appeared at the middle of the screen, which served as the execution cue. The cursor moved down at a fixed rate until it reached the bottom (feedback time). The horizontal movement of the cursor was controlled by the transplanted EEG signal. If the cursor hit the target, the target turned to yellow (hitting in the middle, no target turned to yellow). The whole run lasted a fixed time of 3 minutes. However, the number of trials in each run depended on moving speed of the cursor on vertical axis. Fig.5.6 illustrates screen setting of the basket game. Fig.5.7 shows the experiment protocol in training and testing sessions.

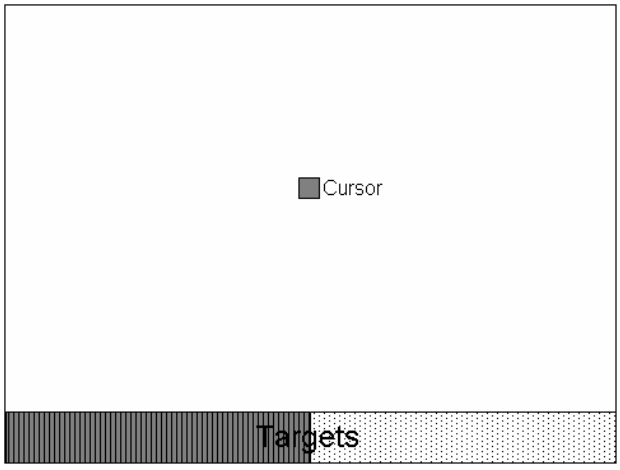

Fig. 5.6. Basket game performed in the online experiment. Subjects controlled horizontal position of the cursor to guide its downward movement to hit one of the two targets at bottom of the screen at a constant speed.

The online experiment consisted of one training session without feedback and one testing sessions with feedback. The number of runs included in one session was different

among the subject. The experiment setup was the same for the training and testing sessions except that there was no horizontal cursor movement in trials of the training session. A 960-ms data segment was picked offline from the averaged training data by an investigator and used to extract the individual TF template and calculate the LDA classifier parameters. In the testing session, the cursor was updated every 80 ms to a new horizontal position (p) according to the following formula:

$$Pt_1 = Pt_0 + S*Clt_1 \quad (5)$$

S was the scaling factor that controlled speed of the cursor horizontal movement. Cl was the classifier output.

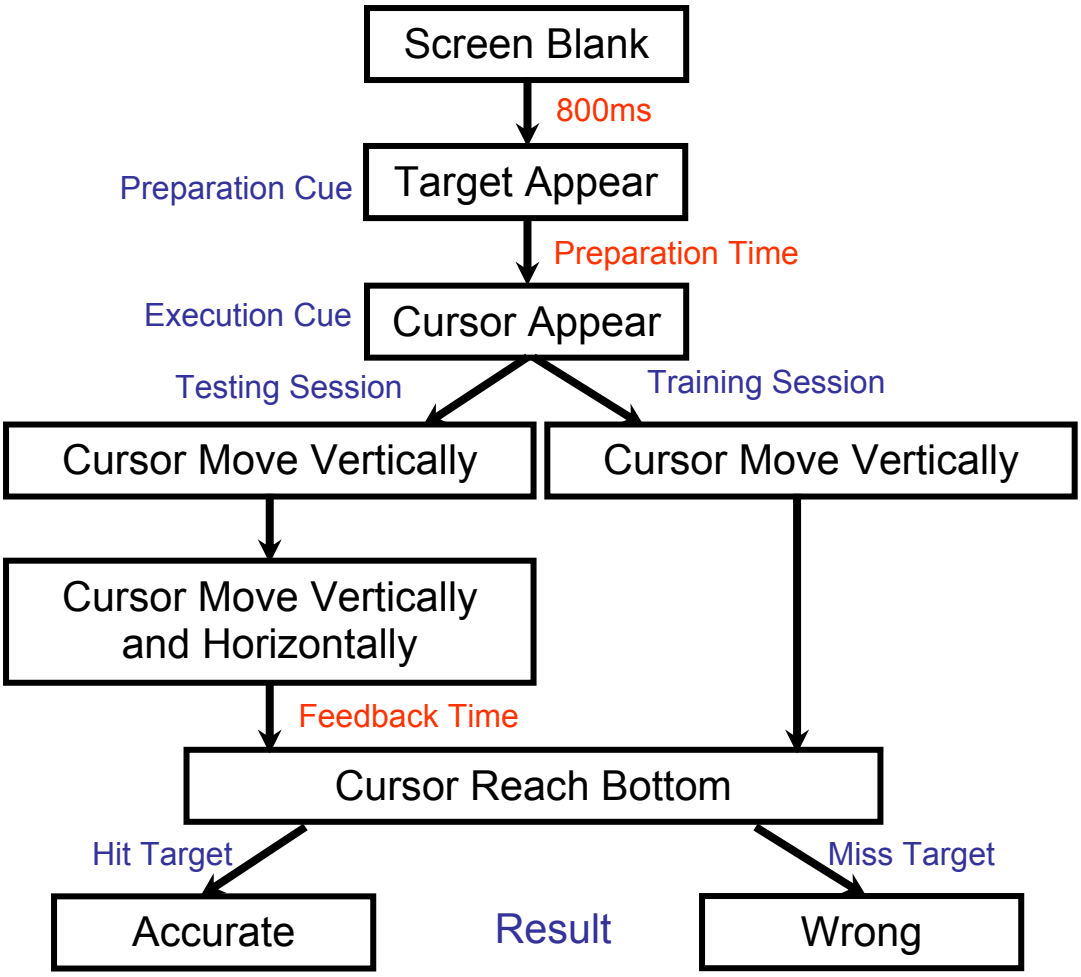

Fig. 5.7. Online experiment protocol for one trial in training and testing session.

In the testing session, at the time (silence time) during initial phase of the feedback period, the cursor horizontal movement was set to 0. The feedback time was the time starting from when the cursor had both horizontal and vertical movements till it hit the bottom. The preparation time, silence time and feedback time were specifically adjusted in each subject according to the actual performance and his/her own choice. We adopted the BCI2000 software (Schalk et al., 2004) infrastructure to build the entire online BCI system and developed our own signal processing module with the time-frequency

template matching algorithms into the signal processing module. The three subjects' experiment parameters are shown in Table I.

	Preparation Time (ms)	Feedback Time (ms)	Trials per Run	Training Session runs	Testing Session runs	S(scaling factor)
Subject1	800	1600	25	3	5	500
Subject2	1600	2000	21	3	5	400
Subject3	3200	2640	16	6	5	300

TABLE I: ONLINE EXPERIMENT PARAMETERS

5.3 Results

5.3.1 Offline Results

The template matching index was acquired according to the described method for the interested time period. Tenfold cross-validation was used to examine the performance of this procedure on nine subjects. Therefore, the data set of each subject was randomly divided into ten sets. The training set (9 out of 10 data sets) was used to get the time-frequency template. The test set (1 out of 10 data sets) was used to calculate the final classification accuracy. This procedure of splitting up the data set, doing the training, and testing the classification accuracy was done ten times on each subject.

The average accuracy was 81.3% for a 4-s EEG data set (0s-4s) and 79.6% for a 3-s time period (0s-3s) (see Table II), better than the results reported in the literatures (Qin and He, 2005, Ince et al., 2006). The average accuracy was 76.8% if only a 2-s data (0s-2s) segment was analyzed, which was still better than the previously reported accuracy.

Accuracy (%)	*S1*	*S2*	*S3*	*S4*	*S5*	*S6*	*S7*	*S8*	*S9*	**AVG**
0-4s	85	92.8	75	69.4	83.3	85	91.1	70.6	79.4	81.3
0-3s	83.3	91.7	75	65	83.9	83.3	88.9	67.8	77.8	79.6
0-2s	81.1	90	72.8	55	79.4	82.8	84.4	66.7	67.2	75.5
0-3s(Qin and He 2005)	72.8	91.7	69.4	68.3	73.9	72.8	81.7	56.7	85.7	74.8
0-4s(Ince et al. 2006)	83.6	92.6	70	70.7	77.8	87.2	89.7	70	83.7	80.6

TABLE II. OFFLINE EXPERIMENT RESULTS

5.3.2 Online Results

The percentage of the accurate trials (the trials that cursor hit the target in the end) out of the total trials in each run of the testing session was used to quantify each subject's performance. The accuracy of each run for each subject was shown on Table III. All the three subjects reached a level of accuracy above 70% at the end of the testing session. Each session included five 3-min runs. The non-feedback training time for each subject was actually quite short. Two subjects had 3 runs of the non-feedback training that lasted totally 9 minutes if the inter-run rest time was not included. One subject had 6 runs of non-feedback training time.

Accuracy	*Run 1*	*Run 2*	*Run 3*	*Run 4*	**Run 5**
Subject1	92%	96%	96%	84%	89%
Subject2	52%	67%	62%	71%	71%
Subject3	69%	56%	69%	69%	75%

TABLE III. ONLINE EXPERIMENT RESULTS

5.4 Discussion

This study utilized both time and frequency information to real-time classify surface EEG signals in an online BCI experiment. The results of the offline and pilot

online experiments demonstrate that the time-frequency features from only two electrodes could discriminate information of motor imaging from non-feedback training to feedback training. In addition, the time-frequency features are robust and efficient discriminators that only need a relatively short period of non-feedback training.

This study employed both time and frequency information to distinguish the left and right hand movement imagery. This method preserves all useful information simultaneously in one time-frequency distribution template for classification. And it is not necessary to pick up any particular frequency bands as several studies used to do (Wolpaw et al., 1991, Wolpaw et al., 2002, Scherer et al., 2003). Specifying the frequency band information may not only require extra complex and reliable algorithm (Scherer et al., 2003) but also lose some useful information in other related frequency bands. The time information of ERD/ERS was usually neglected in real time BCI in the previous real time BCIs. One possible consideration may be that using time information in the real time BCIs may induce big time delay in response to the subject's intention. In our online experiment, 960 ms template was used. So there was 960 ms delay for every feedback update. However, the delay of about one second is not crucial for the simple task when the accuracy is high. The BCI based on AR coefficients of motor imagery EEG data also had one second delay (Pfurtscheller et al., 1998). And the features across 960ms were more reliable than that from tens milliseconds. The possible false trigger caused by the artificial signals could be avoided in this way. Using one second time delay to exchange for more distinguishable and reliable information is worthwhile.

Compared with previous studies, this study achieved more than 70% accuracy only after no more than 18-minutes non-feedback training and 15-minutes feedback testing

time. It is reported that using mu- and beta-frequency components usually need several months to develop high-accuracy cursor control (i.e.,> 90%) (Wolpaw et al., 1991). Using motor imagery based features, an accuracy of 80%-95% can be achieved after 6-10 of 20 minutes training (Pfurtscheller et al., 1998, Guger et al., 1999, Guger et al., 2001). It is noticed that classification accuracies of subject 2 and subject 3 continuously increased as the feedback testing session went on, which indicates a progressive adaptation. Actually, the adaptation is a two-way avenue: user adapting to system and system automatically adapting to the user too. In this study, the users adapted to system via feedback training, which led to more accurate and efficient communication between users and BCI system. If more sessions were tested, the time-frequency template and coefficients of the classifier would be updated with the newest data. In this way the system also adapts itself to each user.

EEG data from only two fixed electrodes was used to detect the motor imagery pattern in this study. The spatial information was limited. While ERD/ERS features are time, frequency and spatial information related. ERD/ERS may be localized in different electrode with motor cortical area in different subject. If the spatial information could be specified for each subject, the classification accuracy would be greatly increased.

A number of personal factors, such as consistent concentration, fatigue, mood, and motivation, can have considerable effect on the training result and should be carefully treated to maximize their positive or minimize negative effects on the result.

Future work will test effects of longer-term feedback training on improving accuracy and information transformation rate. Improving classification accuracy by real time updating template with the newest feedback session data and LDA classifier weights

and incorporating spatial information will be tested. Another important direction of future work includes combining the single trial coherence estimation method described in Chapter 4 into this real time system.

CHAPTER VI

CONCLUSIONS AND FUTURE WORK

This dissertation includes two major parts. The first part reports findings of three studies that examined effects of voluntary muscle fatigue on functional neuromuscular coupling. The aims of the three studies were:

1. To quantify functional corticomuscular coupling change during voluntary fatigue in healthy individuals (Chapter 2).
2. To detect functional corticomuscular coupling impairment in cancer patients with fatigue symptoms (Chapter 3).
3. To explore a technique for detecting functional corticomuscular coupling in short single trial duration (Chapter 4).

An objective neuromuscular index, EEG-EMG coherence, was estimated as a representation of strength of functional corticomuscular coupling during voluntary muscle fatigue. The studies showed a significant reduction of EEG-EMG coherence

during sustained sub-maximal contraction of the elbow flexor muscles in both CRF patients and healthy controls. Another significant result of the study was the weakening of corticomuscular coupling in CRF patients compared to healthy controls within the minimal fatigue stage. The reduction of the coherence do demonstrate the dissociation of brain and muscle signals during fatigue and cancer related fatigue, which provides a new perspective to understand fatigue and cancer related fatigue mechanisms at the system level. The coherence reduction by muscle fatigue in healthy controls is related to the physiological differential effects of fatigue on the central and muscular systems, while the lower coherence level in CRF patients may be caused by the differential effects of central and muscular systems induced by additional pathophysiological impairment in the patients. This explains why normal fatigue can be recovered by rest in healthy people while CRF is a persistent symptom. Given the fact that this is the first report of the coherence reduction, it could be an important addition to the current understanding of neural mechanisms underlying muscle fatigue and CRF and may stimulate interests to pursue the issue further by other investigators. Although significant weakening of the EEG-EMG coherence was detected during muscle fatigue in healthy individuals and in CRF patients in the minimal-fatigue stage (compared with the controls), further information such as whether weakening of the fCMC is a consequence of central or peripheral fatigue could not be revealed by the current coherence analysis. Therefore, many directions of the future research based on findings of this study can be launched, include detecting directional coherence changes to further elucidate weather it is the weakening communication of brain to muscle or muscle to brain during muscle fatigue,

quantifying phase difference of brain signal and corresponding muscle signal during muscle fatigue, and detecting fCMC changes before and after treatment in cancer patients.

The third aim of the first part of the dissertation demonstrated successful use of the wavelet-based single trial coherence estimation method for detecting the fatigue effect on functional corticomuscular coupling in repeated maximal muscle contractions. The coherence decreased significantly from the first half of the repeated-maximal-muscle-contraction task to the second half of the task. The single-trial coherence revealed more detailed information: different subjects have different patterns of coherence reduction with consecutive trials and more detailed dynamic fatigue-related EEG-EMG coherence changes are seen with improved time resolution. This single-trial coherence estimation method also provides the possibility of real time power spectrum and coherence detection that might be used in the future as a cancer related therapy indicator or muscle training index for athletes. A major limitation of the single-trial coherence estimation described in this dissertation is that the time duration of each single trial can not be too short (the time duration requirement is different for different target frequency band analysis, for example, in chapter 4, at least a 2-s data set is needed for 8 Hz and higher frequency wavelet coherence analysis).

The second part of the dissertation describes a real time system that successfully classified surface EEG signals in online BCI experiments utilizing wavelet-based time frequency features. The classified signals can be used to control assisting devices to aid function of patients who are disabled. Future work includes combining this coherence estimation into the online system described in chapter 5 which eventually allow for real

time quantifying coherence and power spectrum of brain and muscle signal changes before, during and after fatigue.

BIBLIOGRAPHY

Abdelmalki, A., Merino, D., Bonneau, D., Bigard, A. X. and Guezennec, C. Y., 1997. Administration of a GABAB agonist baclofen before running to exhaustion in the rat: effects on performance and on some indicators of fatigue. Int J Sports Med. 18, 75-78.

Arihara, M. and Sakamoto, K., 1999. Contribution of motor unit activity enhanced by acute fatigue to physiological tremor of finger. Electromyogr Clin Neurophysiol. 39, 235-247.

Ayoubian Markazi, S., Qazi, S. and Stergioulas, L. K., 2005. Study of Change Blindness EEG Synchronisation using Wavelet Coherence Analysis. Conf Proc IEEE Eng Med Biol Soc. 6, 5995-5998.

Babcock, M. A., Pegelow, D. F., McClaran, S. R., Suman, O. E. and Dempsey, J. A., 1995. Contribution of diaphragmatic power output to exercise-induced diaphragm fatigue. J Appl Physiol. 78, 1710-1719.

Balestra, C., Duchateau, J. and Hainaut, K., 1992. Effects of fatigue on the stretch reflex in a human muscle. Electroencephalogr Clin Neurophysiol. 85, 46-52.

Barnes, E. A. and Bruera, E., 2002. Fatigue in patients with advanced cancer: a review. Int J Gynecol Cancer. 12, 424-428.

Belhaj-Saif, A., Fourment, A. and Maton, B., 1996. Adaptation of the precentral cortical command to elbow muscle fatigue. Exp Brain Res. 111, 405-416.

Bellemare, F. and Garzaniti, N., 1988. Failure of neuromuscular propagation during human maximal voluntary contraction. J Appl Physiol. 64, 1084-1093.

Bigland-Ritchie, B., 1981. EMG/force relations and fatigue of human voluntary contractions. Exerc Sport Sci Rev. 9, 75-117.

Bigland-Ritchie, B., Cafarelli, E. and Vollestad, N. K., 1986. Fatigue of submaximal static contractions. Acta Physiol Scand Suppl. 556, 137-148.

Bigland-Ritchie, B. and Woods, J. J., 1984. Changes in muscle contractile properties and neural control during human muscular fatigue. Muscle Nerve. 7, 691-699.

Blankertz, B., Muller, K. R., Curio, G., Vaughan, T. M., Schalk, G., Wolpaw, J. R., Schlogl, A., Neuper, C., Pfurtscheller, G., Hinterberger, T., Schroder, M. and Birbaumer, N., 2004. The BCI Competition 2003: progress and perspectives in detection and discrimination of EEG single trials. IEEE Trans Biomed Eng. 51, 1044-1051.

Bostanov, V., 2004. BCI Competition 2003--Data sets Ib and IIb: feature extraction from event-related brain potentials with the continuous wavelet transform and the t-value scalogram. IEEE Trans Biomed Eng. 51, 1057-1061.

Bower, J. E., 2006. Management of cancer-related fatigue. Clin Adv Hematol Oncol. 4, 828-829.

Brittain, J. S., Halliday, D. M., Conway, B. A. and Nielsen, J. B., 2007. Single-trial multiwavelet coherence in application to neurophysiological time series. IEEE Trans Biomed Eng. 54, 854-862.

Brown, P., Corcos, D. M. and Rothwell, J. C., 1997. Does parkinsonian action tremor contribute to muscle weakness in Parkinson's disease? Brain. 120 (Pt 3), 401-408.

Brunner, C., Scherer, R., Graimann, B., Supp, G. and Pfurtscheller, G., 2006. Online control of a brain-computer interface using phase synchronization. IEEE Trans Biomed Eng. 53, 2501-2506.

Butler, J. E., Taylor, J. L. and Gandevia, S. C., 2003. Responses of human motoneurons to corticospinal stimulation during maximal voluntary contractions and ischemia. J Neurosci. 23, 10224-10230.

Cella, D., Lai, J. S., Chang, C. H., Peterman, A. and Slavin, M., 2002. Fatigue in cancer patients compared with fatigue in the general United States population. Cancer. 94, 528-538.

Chaudhuri, A. and Behan, P. O., 2004. Fatigue in neurological disorders. Lancet. 363, 978-988.

Chen, C. W., Lin, C. C. and Ju, M. S., 2007. Detecting movement-related EEG change by wavelet decomposition-based neural networks trained with single thumb movement. Clin Neurophysiol. 118, 802-814.

Conway, B. A., Halliday, D. M., Farmer, S. F., Shahani, U., Maas, P., Weir, A. I. and Rosenberg, J. R., 1995. Synchronization between motor cortex and spinal motoneuronal pool during the performance of a maintained motor task in man. J Physiol. 489 (Pt 3), 917-924.

Dimeo, F., Stieglitz, R. D., Novelli-Fischer, U., Fetscher, S., Mertelsmann, R. and Keul, J., 1997. Correlation between physical performance and fatigue in cancer patients. Ann Oncol. 8, 1251-1255.

Donnelly, S. and Walsh, D., 1995. The symptoms of advanced cancer. Semin Oncol. 22, 67-72.

Ebenbichler, G. R., Kollmitzer, J., Erim, Z., Loscher, W. N., Kerschan, K., Posch, M., Nowotny, T., Kranzl, A., Wober, C. and Bochdansky, T., 2000. Load-dependence

of fatigue related changes in tremor around 10 Hz. Clin Neurophysiol. 111, 106-111.

Enoka, R. M. and Stuart, D. G., 1992. Neurobiology of muscle fatigue. J Appl Physiol. 72, 1631-1648.

Feige, B., Aertsen, A. and Kristeva-Feige, R., 2000. Dynamic synchronization between multiple cortical motor areas and muscle activity in phasic voluntary movements. J Neurophysiol. 84, 2622-2629.

Flanders, M., 2002. Choosing a wavelet for single-trial EMG. J Neurosci Methods. 116, 165-177.

Fuglevand, A. J., Bilodeau, M. and Enoka, R. M., 1995. Short-term immobilization has a minimal effect on the strength and fatigability of a human hand muscle. J Appl Physiol. 78, 847-855.

Fuglevand, A. J., Zackowski, K. M., Huey, K. A. and Enoka, R. M., 1993. Impairment of neuromuscular propagation during human fatiguing contractions at submaximal forces. J Physiol. 460, 549-572.

Gandevia, S. C., 2001. Spinal and supraspinal factors in human muscle fatigue. Physiol Rev. 81, 1725-1789.

Gandevia, S. C., Allen, G. M., Butler, J. E. and Taylor, J. L., 1996. Supraspinal factors in human muscle fatigue: evidence for suboptimal output from the motor cortex. J Physiol. 490 (Pt 2), 529-536.

Garland, S. J., 1991. Role of small diameter afferents in reflex inhibition during human muscle fatigue. J Physiol. 435, 547-558.

Garland, S. J. and Kaufman, M. P., 1995. Role of muscle afferents in the inhibition of motoneurons during fatigue. Adv Exp Med Biol. 384, 271-278.

Glassman, E. L., 2005. A wavelet-like filter based on neuron action potentials for analysis of human scalp electroencephalographs. IEEE Trans Biomed Eng. 52, 1851-1862.

Goelz, H., Jones, R. D. and Bones, P. J., 2000. Wavelet analysis of transient biomedical signals and its application to detection of epileptiform activity in the EEG. Clin Electroencephalogr. 31, 181-191.

Guger, C., Schlogl, A., Neuper, C., Walterspacher, D., Strein, T. and Pfurtscheller, G., 2001. Rapid prototyping of an EEG-based brain-computer interface (BCI). IEEE Trans Neural Syst Rehabil Eng. 9, 49-58.

Guger, C., Schlogl, A., Walterspacher, D. and Pfurtscheller, G., 1999. Design of an EEG-based brain-computer interface (BCI) from standard components running in real-time under Windows. Biomed Tech (Berl). 44, 12-16.

Hellwig, B., Haussler, S., Lauk, M., Guschlbauer, B., Koster, B., Kristeva-Feige, R., Timmer, J. and Lucking, C. H., 2000. Tremor-correlated cortical activity detected by electroencephalography. Clin Neurophysiol. 111, 806-809.

Hjorth, B., 1975. An on-line transformation of EEG scalp potentials into orthogonal source derivations. Electroencephalogr Clin Neurophysiol. 39, 526-530.

Ince, N. F., Arica, S. and Tewfik, A., 2006. Classification of single trial motor imagery EEG recordings with subject adapted non-dyadic arbitrary time-frequency tilings. J Neural Eng. 3, 235-244.

Irvine, D. M., Vincent, L., Bubela, N., Thompson, L. and Graydon, J., 1991. A critical appraisal of the research literature investigating fatigue in the individual with cancer. Cancer Nurs. 14, 188-199.

Issartel, J., Marin, L., Gaillot, P., Bardainne, T. and Cadopi, M., 2006. A practical guide to time-frequency analysis in the study of human motor behavior: the contribution of wavelet transform. J Mot Behav. 38, 139-159.

Johnston, J., Rearick, M. and Slobounov, S., 2001. Movement-related cortical potentials associated with progressive muscle fatigue in a grasping task. Clin Neurophysiol. 112, 68-77.

Kalcher, J., Flotzinger, D., Neuper, C., Golly, S. and Pfurtscheller, G., 1996. Graz brain-computer interface II: towards communication between humans and computers based on online classification of three different EEG patterns. Med Biol Eng Comput. 34, 382-388.

Kamousi, B., Liu, Z. and He, B., 2005. Classification of motor imagery tasks for brain-computer interface applications by means of two equivalent dipoles analysis. IEEE Trans Neural Syst Rehabil Eng. 13, 166-171.

Kilner, J. M., Baker, S. N., Salenius, S., Hari, R. and Lemon, R. N., 2000. Human cortical muscle coherence is directly related to specific motor parameters. J Neurosci. 20, 8838-8845.

Kilner, J. M., Baker, S. N., Salenius, S., Jousmaki, V., Hari, R. and Lemon, R. N., 1999. Task-dependent modulation of 15-30 Hz coherence between rectified EMGs from human hand and forearm muscles. J Physiol. 516 (Pt 2), 559-570.

Klein, A., Sauer, T., Jedynak, A. and Skrandies, W., 2006. Conventional and wavelet coherence applied to sensory-evoked electrical brain activity. IEEE Trans Biomed Eng. 53, 266-272.

Kristeva, R., Patino, L. and Omlor, W., 2007. Beta-range cortical motor spectral power and corticomuscular coherence as a mechanism for effective corticospinal interaction during steady-state motor output. Neuroimage.

Lachaux, J. P., Lutz, A., Rudrauf, D., Cosmelli, D., Le Van Quyen, M., Martinerie, J. and Varela, F., 2002. Estimating the time-course of coherence between single-trial brain signals: an introduction to wavelet coherence. Neurophysiol Clin. 32, 157-174.

Leao, R. N. and Burne, J. A., 2004. Continuous wavelet transform in the evaluation of stretch reflex responses from surface EMG. J Neurosci Methods. 133, 115-125.

Lee, D., 2002. Analysis of phase-locked oscillations in multi-channel single-unit spike activity with wavelet cross-spectrum. J Neurosci Methods. 115, 67-75.

Lemm, S., Blankertz, B., Curio, G. and Muller, K. R., 2005. Spatio-spectral filters for improving the classification of single trial EEG. IEEE Trans Biomed Eng. 52, 1541-1548.

Leonard, C. T., Kane, J., Perdaems, J., Frank, C., Graetzer, D. G. and Moritani, T., 1994. Neural modulation of muscle contractile properties during fatigue: afferent feedback dependence. Electroencephalogr Clin Neurophysiol. 93, 209-217.

Li, X., Yao, X., J, G. J. and Fox, J., 2005. Computational Neuronal Oscillations using Morlet Wavelet Transform. Conf Proc IEEE Eng Med Biol Soc. 2, 2009-2012.

Liu, J. Z., Dai, T. H., Elster, T. H., Sahgal, V., Brown, R. W. and Yue, G. H., 2000. Simultaneous measurement of human joint force, surface electromyograms, and functional MRI-measured brain activation. J Neurosci Methods. 101, 49-57.

Liu, J. Z., Lewandowski, B., Karakasis, C., Yao, B., Siemionow, V., Sahgal, V. and Yue, G. H., 2007. Shifting of activation center in the brain during muscle fatigue: an explanation of minimal central fatigue? Neuroimage. 35, 299-307.

Liu, J. Z., Shan, Z. Y., Zhang, L. D., Sahgal, V., Brown, R. W. and Yue, G. H., 2003. Human brain activation during sustained and intermittent submaximal fatigue muscle contractions: an FMRI study. J Neurophysiol. 90, 300-312.

Liu, J. Z., Yao, B., Siemionow, V., Sahgal, V., Wang, X., Sun, J. and Yue, G. H., 2005. Fatigue induces greater brain signal reduction during sustained than preparation phase of maximal voluntary contraction. Brain Res. 1057, 113-126.

Liu, J. Z., Zhang, L., Yao, B., Sahgal, V. and Yue, G. H., 2005. Fatigue induced by intermittent maximal voluntary contractions is associated with significant losses in muscle output but limited reductions in functional MRI-measured brain activation level. Brain Res. 1040, 44-54.

Liu, J. Z., Zhang, L., Yao, B. and Yue, G. H., 2002. Accessory hardware for neuromuscular measurements during functional MRI experiments. Magma. 13, 164-171.

Lovett, E. G. and Ropella, K. M., 1997. Time-frequency coherence analysis of atrial fibrillation termination during procainamide administration. Ann Biomed Eng. 25, 975-984.

Marsden, J. F., Werhahn, K. J., Ashby, P., Rothwell, J., Noachtar, S. and Brown, P., 2000. Organization of cortical activities related to movement in humans. J Neurosci. 20, 2307-2314.

Merzagora, A. C., Bunce, S., Izzetoglu, M. and Onaral, B., 2006. Wavelet analysis for EEG feature extraction in deception detection. Conf Proc IEEE Eng Med Biol Soc. 1, 2434-2437.

Mima, T. and Hallett, M., 1999. Corticomuscular coherence: a review. J Clin Neurophysiol. 16, 501-511.

Mima, T., Toma, K., Koshy, B. and Hallett, M., 2001. Coherence between cortical and muscular activities after subcortical stroke. Stroke. 32, 2597-2601.

Mock, V., Atkinson, A., Barsevick, A., Cella, D., Cimprich, B., Cleeland, C., Donnelly, J., Eisenberger, M. A., Escalante, C., Hinds, P., Jacobsen, P. B., Kaldor, P., Knight, S. J., Peterman, A., Piper, B. F., Rugo, H., Sabbatini, P. and Stahl, C., 2000. NCCN Practice Guidelines for Cancer-Related Fatigue. Oncology (Williston Park). 14, 151-161.

Monga, U., Jaweed, M., Kerrigan, A. J., Lawhon, L., Johnson, J., Vallbona, C. and Monga, T. N., 1997. Neuromuscular fatigue in prostate cancer patients undergoing radiation therapy. Arch Phys Med Rehabil. 78, 961-966.

Morrow, G. R., Shelke, A. R., Roscoe, J. A., Hickok, J. T. and Mustian, K., 2005. Management of cancer-related fatigue. Cancer Invest. 23, 229-239.

Neuper, C., Schlogl, A. and Pfurtscheller, G., 1999. Enhancement of left-right sensorimotor EEG differences during feedback-regulated motor imagery. J Clin Neurophysiol. 16, 373-382.

Parra, L., Alvino, C., Tang, A., Pearlmutter, B., Yeung, N., Osman, A. and Sajda, P., 2002. Linear spatial integration for single-trial detection in encephalography. Neuroimage. 17, 223-230.

Peltier, S. J., LaConte, S. M., Niyazov, D. M., Liu, J. Z., Sahgal, V., Yue, G. H. and Hu, X. P., 2005. Reductions in interhemispheric motor cortex functional connectivity after muscle fatigue. Brain Res. 1057, 10-16.

Perez, D., Helbig, M., Kirlangic, M. and Ivanova, G., 2005. Comparison of time-variant coherence algorithms in single-trial: a dynamic analysis. Conf Proc IEEE Eng Med Biol Soc. 6, 5647-5650.

Pfurtscheller, G., Neuper, C., Schlogl, A. and Lugger, K., 1998. Separability of EEG signals recorded during right and left motor imagery using adaptive autoregressive parameters. IEEE Trans Rehabil Eng. 6, 316-325.

Pfurtscheller, G., Stancak, A., Jr. and Neuper, C., 1996. Event-related synchronization (ERS) in the alpha band--an electrophysiological correlate of cortical idling: a review. Int J Psychophysiol. 24, 39-46.

Qin, L., Ding, L. and He, B., 2004. Motor imagery classification by means of source analysis for brain-computer interface applications. J Neural Eng. 1, 135-141.

Qin, L. and He, B., 2005. A wavelet-based time-frequency analysis approach for classification of motor imagery for brain-computer interface applications. J Neural Eng. 2, 65-72.

Rosenberg, J. R., Amjad, A. M., Breeze, P., Brillinger, D. R. and Halliday, D. M., 1989. The Fourier approach to the identification of functional coupling between neuronal spike trains. Prog Biophys Mol Biol. 53, 1-31.

Sajda, P., Gerson, A., Muller, K. R., Blankertz, B. and Parra, L., 2003. A data analysis competition to evaluate machine learning algorithms for use in brain-computer interfaces. IEEE Trans Neural Syst Rehabil Eng. 11, 184-185.

Salenius, S., Avikainen, S., Kaakkola, S., Hari, R. and Brown, P., 2002. Defective cortical drive to muscle in Parkinson's disease and its improvement with levodopa. Brain. 125, 491-500.

Samar, V. J., 1999. Wavelet analysis of neuroelectric waveforms. Brain Lang. 66, 1-6.

Schalk, G., McFarland, D. J., Hinterberger, T., Birbaumer, N. and Wolpaw, J. R., 2004. BCI2000: a general-purpose brain-computer interface (BCI) system. IEEE Trans Biomed Eng. 51, 1034-1043.

Scherer, R., Graimann, B., Huggins, J. E., Levine, S. P. and Pfurtscheller, G., 2003. Frequency component selection for an ECoG-based brain-computer interface. Biomed Tech (Berl). 48, 31-36.

Senhadji, L., Dillenseger, J. L., Wendling, F., Rocha, C. and Kinie, A., 1995. Wavelet analysis of EEG for three-dimensional mapping of epileptic events. Ann Biomed Eng. 23, 543-552.

Servaes, P., Verhagen, C. and Bleijenberg, G., 2002. Fatigue in cancer patients during and after treatment: prevalence, correlates and interventions. Eur J Cancer. 38, 27-43.

Sidaway, B. and Trzaska, A. R., 2005. Can mental practice increase ankle dorsiflexor torque? Phys Ther. 85, 1053-1060.

Sogaard, K., Gandevia, S. C., Todd, G., Petersen, N. T. and Taylor, J. L., 2006. The effect of sustained low-intensity contractions on supraspinal fatigue in human elbow flexor muscles. J Physiol. 573, 511-523.

Sood, A. and Moynihan, T. J., 2005. Cancer-related fatigue: an update. Curr Oncol Rep. 7, 277-282.

Stone, P., Richards, M. and Hardy, J., 1998. Fatigue in patients with cancer. Eur J Cancer. 34, 1670-1676.

Tallon-Baudry, C., Bertrand, O., Delpuech, C. and Permier, J., 1997. Oscillatory gamma-band (30-70 Hz) activity induced by a visual search task in humans. J Neurosci. 17, 722-734.

Tanino, Y., Daikuya, S., Nishimori, T., Takasaki, K. and Suzuki, T., 2003. M wave and H-reflex of soleus muscle before and after electrical muscle stimulation in healthy subjects. Electromyogr Clin Neurophysiol. 43, 381-384.

Taylor, J. L., Butler, J. E. and Gandevia, S. C., 2000. Changes in muscle afferents, motoneurons and motor drive during muscle fatigue. Eur J Appl Physiol. 83, 106-115.

Taylor, J. L. and Gandevia, S. C., 2001. Transcranial magnetic stimulation and human muscle fatigue. Muscle Nerve. 24, 18-29.

Taylor, J. L., Todd, G. and Gandevia, S. C., 2006. Evidence for a supraspinal contribution to human muscle fatigue. Clin Exp Pharmacol Physiol. 33, 400-405.

Tecchio, F., Porcaro, C., Zappasodi, F., Pesenti, A., Ercolani, M. and Rossini, P. M., 2006. Cortical short-term fatigue effects assessed via rhythmic brain-muscle coherence. Exp Brain Res. 174, 144-151.

Torrence, C. a. W., P, 1999. Interdecadal changes in the enso-mon-soon system. J Climatol. 12, 2679-2690.

van Duinen, H., Renken, R., Maurits, N. and Zijdewind, I., 2007. Effects of motor fatigue on human brain activity, an fMRI study. Neuroimage. 35, 1438-1449.

Volkmann, J., Joliot, M., Mogilner, A., Ioannides, A. A., Lado, F., Fazzini, E., Ribary, U. and Llinas, R., 1996. Central motor loop oscillations in parkinsonian resting tremor revealed by magnetoencephalography. Neurology. 46, 1359-1370.

Walsh, D., Donnelly, S. and Rybicki, L., 2000. The symptoms of advanced cancer: relationship to age, gender, and performance status in 1,000 patients. Support Care Cancer. 8, 175-179.

Wolpaw, J. R., Birbaumer, N., McFarland, D. J., Pfurtscheller, G. and Vaughan, T. M., 2002. Brain-computer interfaces for communication and control. Clin Neurophysiol. 113, 767-791.

Wolpaw, J. R., McFarland, D. J., Neat, G. W. and Forneris, C. A., 1991. An EEG-based brain-computer interface for cursor control. Electroencephalogr Clin Neurophysiol. 78, 252-259.

Xiao, S. and Leung, S. C., 1997. Muscle fatigue monitoring using wavelet decomposition of surface EMG. Biomed Sci Instrum. 34, 147-152.

Xu, Y., Haykin, S. and Racine, R. J., 1999. Multiple window time-frequency distribution and coherence of EEG using Slepian sequences and hermite functions. IEEE Trans Biomed Eng. 46, 861-866.

Yavuzsen, T., Ranganathan, D. M., Siemionow, V., Walsh, V., Kirkova, D., Khoshknab, J., Lagman, D., LeGrand, R. S, Yue, G.H., Cancer related fatigue: Central or peripheral? J Clin Oncol. Submitted.

Yang, Q., Fang, Y., Siemionow, V., Khoshknabi, D., Davis, M.P., Sahgal, V., Yue, G. H., Weakening of corticomuscular signal coupling during muscle fatigue. J Clin Neurophysi. Submitted.

Yang, Q., Fang, Y., Siemionow, V., Yue, G. H., Online and Offline Implementation of Time-frequency Template Matching Method for Classifying Motor Imagery in Brain Computer Interface. Proc. of Joint Meeting of 6th International Symposium on Noninvasive Functional Source Imaging of Brain and Heart and International Conference on Functional Biomedical Imaging (NFSI&ICFBI'07). 78 - 81, 2007

Yue, G. H., Bilodeau, M., Hardy, P. A. and Enoka, R. M., 1997. Task-dependent effect of limb immobilization on the fatigability of the elbow flexor muscles in humans. Exp Physiol. 82, 567-592.

Zhan, Y., Halliday, D., Jiang, P., Liu, X. and Feng, J., 2006. Detecting time-dependent coherence between non-stationary electrophysiological signals--a combined statistical and time-frequency approach. J Neurosci Methods. 156, 322-332.

APPENDIX

Appendix A

Abbreviations:

ALS: Amyotrophic lateral sclerosis
AR: Autoregressive model
BB: Biceps brachii
BCI: Brain-computer interface
BR: Brachioradialis
CRF: Cancer related fatigue
CSP: Common spatial patterns
DSLVQ: Distinction sensitive learning vector quantizier
ED: Extensor digitorum
FDP: Flexor digitorum profundus
FDS: Flexor digitorum superficialis
EEG: Electroencephalography
EMG: Electromyography
ERD: Event-related de-synchronization
ERS: Event-related synchronization
ERP: Event-related potential
FFT: Fast Fourier transform
fMRI: Functional Magnetic Resonance Imaging
fCMC: functional corticomuscular coupling
ICA: Independent component analysis
IIR: Impulse response filter
kNN: k-nearest-neighbor
LDA: Linear discriminant analysis
MEG: Magnetoencephalography
MRCP: Motor cortical related potential
MRI: Magnetic Resonance Imaging
MVAR: Multivariate autoregressive coefficients
MVC: Maximal voluntary contraction
PSD: Power spectral density
SNR: Signal to noise ratio
SSVER: Steady-state visual evoked response
SVM: Support vector machine
TB: Triceps brachii
TF: Time-frequency
VEP: Visual evoked potential